de Vilder Saskia (Orcid ID: 0000-0002-4531-2070)

Controls on the geotechnical response of sedimentary rocks to weathering

de Vilder, S.J[1,2*]., Brain, M.J[1]., Rosser, N.J[1]

Department of Geography, Durham University, Lower Mountjoy, South Road, Durham DH1 3LE UK

[2] Now at GNS Science, 1 Fairway Drive, Avalon 5010, NZ

*Corresponding author: s.devilder@gns.cri.nz

Keywords: unconfined compression, rock strength, stress history, failure style, rockfall, rock bridges

This article has been accepted for publication and undergone full peer review but has not been through the copyediting, typesetting, pagination and proofreading process which may lead to differences between this version and the Version of Record. Please cite this article as doi: 10.1002/esp.4619

Abstract

Weathering reduces the strength of rocks and so is a key control on the stability of rock slopes. Recent research suggests that the geotechnical response of rocks to weathering varies with ambient stress conditions resulting from overburden loading and/or stress concentrations driven by near-surface topography. In addition, the stress history experienced by the rock can influence the degree to which current weathering processes cause rock breakdown. To address the combined effect of these potential controls, we conducted a set of weathering experiments on two sedimentary lithologies in laboratory and field conditions. We firstly defined the baseline geotechnical behaviour of each lithology, characterising surface hardness and stress-strain behaviour in unconfined compression. Weathering significantly reduced intact rock strength, but this was not evident in measurements of surface hardness. The ambient compressive stress applied to samples throughout the experiments did not cause any observable differences in the geotechnical behaviour of the samples. We created a stress history effect in sub-sets of samples by generating a population of microcracks that could be exploited by weathering processes. We also geometrically modified groups of samples to cause near-surface stress concentrations that may allow greater weathering efficacy. However, even these pronounced sample modifications resulted in insignificant changes in geotechnical behaviour when compared to unmodified samples. The observed reduction in rock strength changed the nature of failure of the samples, which developed post-peak strength and underwent multiple stages of brittle failure. Although weakened, these samples could sustain greater stress and strain following exceedance of peak strength. On this basis, the multi-stage failure style exhibited by

weaker weathered rock may permit smaller-magnitude, higher-frequency events to trigger fracture through intact rock bridges as well as influencing the characteristics of pre-failure deformation. These findings are consistent with patterns of behaviour observed in field monitoring results.

Introduction

Rock slope failures are a significant hazard (Dussauge-Peisser et al., 2002; Fell et al., 2008; Guzzetti et al., 1999) and contribute to landscape evolution over a variety of timescales (Clarke and Burbank, 2010; Korup et al., 2007; Moore et al., 2009). The susceptibility of a rock slope to failure is controlled by its intrinsic properties, such as the strength of intact rock bridges (Jennings, 1970), the nature of joint sets (Einstein et al., 1983; Goodman and Shi, 1985), and its physical setting (slope angle, aspect and curvature) (e.g. Matsuoka and Sakai, 1999; Messenzehl et al., 2017; Sass, 2005). Slopes can be destabilised rapidly in response to sudden and short-lived changes in stress conditions that trigger failure, such as those resulting from strong earthquake ground shaking or heavy rainfall (Iverson, 2000; Keefer et al., 1987). Rock slope instability can also develop over longer (10^0 - 10^3 years) timescales in response to incremental and cumulative reductions in rock mass strength driven by micro-fracture development and/or weathering processes that reduce the cohesional strength of rocks (Collins and Stock, 2016; Eppes and Keanini, 2017; Gunzburger et al., 2005).

The significance of weathering in modifying rock strength has been widely observed in a number of studies (e.g. Durgin, 1977; Fookes et al., 1988; Hencher and

McNicholl, 1995; Migon, 2010; Thomson et al., 2014; Yatsu, 1988) and its importance for rock slope stability has been demonstrated in numerical and analogue studies (e.g. Bachmann et al., 2004; Huisman et al., 2011). Engineering classifications provide descriptive insight into the nature of weathering along discontinuities (e.g. Selby, 1980; Hoek, 1983), but such schemes do not sufficiently consider weathering-induced strength degradation of intact rock bridges that critically influence shallow rock slope failures and rockfall activity, which are our focus here (de Vilder et al., 2017; Jennings, 1970; Kemeny, 2005). Weathering processes operate concurrently and/or interact with a range of other processes that prepare slopes for macro-scale fracture (Aldred et al., 2016; Atkinson, 1984; Collins and Stock, 2016; Eppes and Keanini, 2017b; Eppes et al., 2016; Gischig et al., 2011; Lamp et al., 2017; Rosser et al., 2013; Stock et al., 2012) but their combined effect on rock mass strength and failure style remains poorly constrained.

Laboratory experiments have improved our understanding of weathering processes and their influence on surficial changes to rocks (Goudie, 2016; e.g. Moses et al., 2014). However, these studies are not sufficient to fully constrain the influence of weathering on changing intact rock strength and rock slope stability for a variety of reasons. Firstly, few of these studies consider changes in rock strength at a scale relevant to rock slope failures, particularly for small and shallow rockfalls where stability is controlled by one critical rock bridge (de Vilder et al., 2017). Secondly, weathering can also cause changes to rock rheology (Fookes et al., 1988). In turn, this may result in a change in the nature and style of failure (Basu et al., 2009; Gupta and Seshagiri Rao, 2000; Viles, 2013). This aspect of rock response is rarely directly considered in weathering studies. Thirdly, conventional weathering studies

undertaken under laboratory conditions replicate environments where ambient compressive, shear or tensile stress conditions are considered negligible, such as desert surfaces or foreshore platforms (e.g. Coombes et al., 2013; Mottershead, 2013; Viles, 2005; Warke, 2007). However, stress concentrations resulting from temporal and spatial variations in topography, overburden load and macro- and local-scale slope geometry (Brain et al., 2014; Leith et al., 2014a, 2014b; Martel, 2006) can occur in rock slopes. In turn, these elevated stress conditions can cause, for example, an increased density of microcracks (Eberhardt et al., 1998) that can subsequently be exploited by weathering processes. Recent analogue experiments have suggested that the effects of weathering on rock mass strength may differ where 'ambient' stress concentrations exist (Bruthans et al., 2014; Rihosek et al., 2016; Zhang et al., 2015). Fourthly, the significance of stress history on weathering rates and effects has only recently been directly considered (e.g. Røyne et al., 2008; Viles et al., 2018; Warke, 2007). Viles et al. (2018), for example, demonstrated that rocks that have previously been exposed to physical and chemical weathering processes may be more susceptible to weathering than rocks with no previous stress history. However, this effect has not been considered in the context of potential rheological changes and stress concentrations noted above.

To improve our understanding of the links between weathering and shallow rock slope failure, we undertook a suite of experiments that subjected cylindrical rock samples to weathering processes typically experienced by coastal rock cliffs. Our experimental design allowed us to determine the effects, if any, of ambient compressive stresses on the nature of weathering and its effect(s) on rock strength and failure style. Within our experimental program, we also assessed the influence of

stress history, via generating pre-existing microcrack populations, and stress concentrations, via modifying sample geometries, on the strength and deformation behaviour of rock.

Materials and methods

Sample lithology

We used two lithologies in our study: Staithes Formation Siltstone ('siltstone') and Catcastle Buff Sandstone ('sandstone') (Figure 1). These rocks have different grain size characteristics, strength properties and, hence, associated differences in their potential susceptibility to weathering-driven weakening (cf. Eberhardt et al., 1999). The Siltstone forms part of the Lower Jurassic Staithes sandstone formation, which were deposited within the shallow seas of the Cleveland Basin (Rawson and Wright, 2000). It is light grey-blue, with 2 mm to 6 mm thick banding inclined at 6° to 15° (classification based on ISRM, 2015). The Catcastle Buff Sandstone forms part of the Carboniferous Millstone Grit Group, deposited via fluvial processes in the Central Pennine sub-basin (BGS, 2017). It is light grey-brown, massive and medium grained with minor (≤10%) coarse grains (ISRM, 2015).

Overview and experimental design

The first stage of our experimental program involved determining the baseline geotechnical characteristics of the siltstone and sandstone lithologies. We provide an overview to describe the context and rationale of our experimental design, and then provide details on the specific methods applied in the subsequent sections (these

include; unconfined compression strength testing, sample modification, surface hardness measurements and visual appearance, baseline characterisation, laboratory and field weathering experiments).

To assess changes in intact rock strength, we determined the unconfined compressive strength (UCS) of samples. UCS is a widely-used measurement of strength in rock mechanics and slope engineering (e.g. Jaeger et al., 2007), and also is closely related to other key measurements of intact rock strength (Perras and Diederichs, 2014). UCS testing also allowed us to obtain a detailed understanding of stress-strain and, hence, fundamental rheological behaviour of the sample, including the nature of failure. For the latter, we considered the strain value coincident with peak strength (UCS); we term this ‘strain-at-failure’. In addition, we also noted the number and nature of failure ‘events' that occurred until near or total strength loss had occurred in each sample. These failure events were defined in stress-strain curves as substantial, near-instantaneous reductions in recorded compressive stress with no or limited strain accumulation evident

For our baseline dataset, we used cylindrical samples that are typical of standard geotechnical testing procedures (ASTM, 2008). These standard, unmodified samples are henceforth referred to as *U* (unmodified) samples. We also measured the surface hardness of samples used for baseline characterisation, since this has been used as an indication of rock strength (Aoki and Matsukura, 2007).

To consider the influence of stress history on susceptibility to weathering processes, rates and associated changes in behaviour (Røyne et al., 2008; Viles et al., 2018; Warke, 2007), we pre-loaded a separate set of samples to a predetermined value of

UCS (observed in baseline tests – see results) that was sufficient to cause micro-cracking, but insufficient to cause full failure. This created an elevated density of micro-cracks (and so the stress history, or damage condition). We refer to these 'pre-damaged' samples using the notation *P*.

To consider the effects that variations in cliff-face surface topography and resultant stress concentrations may have on the effectiveness of weathering processes, we cut vertical notches into cylindrical samples and characterised their baseline behaviour. This allowed us to assess if resultant stress concentrations in the areas surrounding these notches created any evidence that resultant enhanced micro-cracking can be subsequently exploited by weathering processes (Lajtai and Lajtai, 1974). In addition, the increase in surface area of the sample as a result of the notch may affect the nature, rate and effectiveness of weathering (Robinson et al., 1982). Samples with modified geometry are referred to using the notation *G*. We considered the combined effects of both modified geometry (notches) and stress history on susceptibility to weathering using a combination of the pre-treatment types outlined above; these are referred to as *PG* samples.

The second stage of our testing program involved assessing the effects of weathering on the key geotechnical properties determined in our baseline characterisation stage, namely strength and rheological behaviour. There were two elements to our experiments. Firstly, we considered the effects of weathering in a controlled laboratory environment. These tests focussed on the effects of salt-water wetting and drying cycles on rock properties, typical of conditions experienced in coastal rock slopes (Mottershead, 2013). Secondly, since weathering processes do

not operate in isolation (Viles, 2013), we also undertook a set of field-based weathering experiments where rock samples were exposed to weather conditions at a coastal cliff-top location in Staithes, North Yorkshire, UK.

For both laboratory and field experiments, we considered the effects of weathering on *U*, *G*, *P* and *PG* samples. In addition, our experimental design allowed us to assess the effects of an elevated ambient compressive stress on weathering impacts on *U*, *G*, *P* and *PG* samples. To do so, we placed samples under a constant vertical compressive stress for the full duration of the experiments in both laboratory and field weathering experiments. The magnitude of compressive stress was selected to be representative of the stress conditions experienced at the base of the coastal cliffs of North Yorkshire. For every sample placed under stress, there was an equivalent control sample that was not subjected to vertical stresses but had been subjected to the same pre-test modifications.

Unconfined compression tests

We determined the UCS of samples in broad accordance with ASTM D7012-14 (2014) using a compressive load frame manufactured by GDS Instruments Ltd. (Barla et al., 2010). Deviations from this standard reflect our experimental design, which involved modifications of sample geometry. For the banded siltstone formation, cores were drilled perpendicular to banding. Samples were loaded under compressive strain control at a rate of 0.1% min^{-1}; this strain rate reflects the net strain recorded by the apparatus and is comprised of both deformation of the rock sample and the apparatus itself in response to load ('net strain'). The magnitude of deformation of the apparatus is constant for a given applied stress. As such, we

could directly compare strain values between samples using net strain. This was an important consideration because use of direct, local measurements of rock sample deformation were not always possible following completion of weathering tests, where the fragile and highly-friable nature of the weathered core surface prevented appropriate attachment of 'local' displacement transducers (LVDTs). However, for all baseline samples and for suitable post-weathering samples, we directly monitored sample deformation using two vertically-mounted and diametrically-opposed LVDTs on the rock surface. Local strain measurements were used to calculate Young's Modulus of Elasticity and characterise the local stress-strain behaviour of the rock (ASTM D7012-14, 2014).

We normalised stress-stain curves relative to the mean value of UCS and net strain at failure of the baseline UCS tests, due to the inherent variability in UCS and strain behaviour in the baseline dataset, and the need to compare baseline tests with weathered samples. Normalised stress and strain values of 1 are equal to the mean values recorded in baseline tests. Normalised axial strain values above and below 1 indicate increases and decreases, respectively, in strain values at failure relative to those observed in baseline tests.

Sample modifications

We created pre-existing damage within the samples by loading designated *P* samples in unconfined compression to 75% of the median UCS observed in standard baseline tests (see results). This magnitude of loading was chosen as it typically considered to exceed the crack initiation threshold, c_i, and, hence generate a population of distributed micro-cracks, but without causing macro-scale fracture

(Figure 2 a) (Eberhardt et al., 1998). For *G*-type samples, we cut three 5 mm wide by 5 mm deep vertical 'notches' spaced 50 mm apart at a 120° circumferential offset between notches (Figure 2 b). The reduction in cross-sectional area was accounted for in the calculation of compressive stress. *PG*-type samples were firstly modified in terms of geometry and then pre-damaged using the same procedures as above.

Surface hardness measurements and visual appearance

We measured baseline surface hardness of samples using a standard (d-type) Equotip portable hardness testing device (Viles et al., 2011). We measured the surface hardness of the rock in Leeb numbers (*L)*; a higher *L* value indicates a greater rock surface hardness. For each sample, we recorded the mean of ten measurements, obtained at random locations on the sample. At the end of each weathering experiment the samples were air dried and then weighed to determine if mass loss or mass gain had occurred. Additionally, we recorded qualitative descriptions and photographs of the condition of each sample, noting how the surface texture and colour changed through time

Baseline characterisation

We determined baseline UCS and stress-strain behaviour of standard (*U*) siltstone (n = 12) and sandstone (n = 11) samples. We also measured baseline UCS and stress-strain behaviour of modified geometry *(G*) samples for siltstone (n = 2) and sandstone (n = 3). All baseline samples were instrumented with two axial LVDTs to record the axial strain response of the samples.

Laboratory weathering experiments

Laboratory weathering experiments were undertaken in a climate-controlled laboratory (temperature: 20.9˚C ± 0.24 ˚C; relative humidity: 45% ± 5.3%), allowing us to isolate the effects of saltwater wetting and drying on the samples. We subjected 32 (16 sandstone and 16 siltstone) rock samples to laboratory-controlled weathering conditions for a total of 90 days. All samples experienced 360 wetting and drying cycles. A summary of sample types considered (*U*, *P*, *G* or *PG*) is provided in Table 1. For each type, vertical compressive stress was applied to two samples, and two samples acted as control (non-stressed) samples that experienced the same weathering cycles, allowing us to isolate the effects of ambient compressive stress on weathering.

We used front-loading oedometers (Head and Epps, 2011, Figure 3) to place appropriate samples under a constant vertical compressive stress of 3.8 MPa, equivalent to approximately 150 m to 200 m of vertical overburden. For the siltstone, this compressive stress represented 11.1% of mean UCS, and for the sandstone 6.8% of mean UCS. Using the pump system detailed in Figure. 3, rock samples were subjected to six-hour wetting and drying cycles consisting of 30 minutes of submersion in sodium chloride solution (200 g/l), followed by drainage of the cell and subsequent exposure to air for 5.5 hours. These six-hour cycles mimic semi-diurnal tidal flooding conditions experienced at the coastal cliff toe at Boulby. We monitored the net vertical deformation of the four ‘stressed’ samples with LVDTs (Figure 3). Vertical displacement of each sample was recorded as the mean of measurements observed over a one-minute interval. We also monitored the surface appearance and

texture of rock samples and measured surface hardness using the Equotip device on a weekly basis.

Following completion of the weathering experiments, we measured the mass of the air-dried samples. We then determined the UCS and associated stress-strain behaviour of all 32 samples. This allowed us to quantify any resultant changes in strength and failure style in response to weathering and in terms of each sample type (*U*, *P*, *G* or *PG*). Half (n = 16) of these samples were instrumented with two axially-mounted LVTDs to characterise local strain; one specimen of each pre-treatment type was selected for LVDT instrumentation. For the remaining half (n = 16) only net strain values were obtained.

Field weathering experiments

We undertook a year-long (19th August 2016 – 30th August 2017) field experiment in which we used a purpose-built loading frame at the cliff top at Boulby, North Yorkshire, UK (Figure 4) to subject 32 (16 sandstone and 16 siltstone) rock samples to cliff-top field conditions. The length of time for the field experiments was longer than that of the laboratory experiments, as the samples were subject to a variety of natural environmental cycles rather than the increased frequency of the saline brine wetting and drying compared to tidal cycles. Based on data collected 3 km to the north at Loftus (Meteorological Office weather station), our field site experiences mean annual precipitation of 467 mm; peak rainfall intensities reach 79.1 mm hr^{-1}. In 2016, mean daily air temperature ranged from -1.99°C in January to 21.0°C in September. However, the potential for frost weathering was limited, with only one day recording a mean daily temperature below freezing.

A summary of the type of samples tested (*U*, *P*, *G* or *PG*) is detailed in Table 1. For each type, a vertical compressive stress of 2 MPa, equivalent to approximately 80 m to 100 m of vertical overburden, was applied to two samples using the loading frame, and two samples acted as non-stressed control samples that experienced the same environmental conditions. The 2 MPa vertical compressive stress was equivalent to 5.9% of mean UCS for siltstone samples, and 3.6% of mean UCS for sandstone samples. During the field experiment, we qualitatively monitored and described the surface appearance and texture of rock samples and measured surface strength using the Equotip device monthly.

Following completion of the field experiments, we measured the post-test mass and bulk density of the samples. We then determined the UCS and associated stress-strain behaviour of all 32 samples. Half (n = 16) of these samples were instrumented with two axially-mounted LVTDs to characterise local strain; one specimen of each pre-treatment type was selected for LVDT instrumentation. For the remaining half (n = 16) only net strain values were obtained.

Analysis Methods

To determine the effects of weathering on rock strength and failure style, we grouped and compared samples based on:

- Lithology: siltstone or sandstone;
- Experimental setting: laboratory or field;
- Ambient compressive stress conditions: ‘control’ (non-stressed) or ‘stressed’ samples; and
- Pre-treatment type: *U*, *P*, *G* or *PG*.

We tested for statistically-significant differences groups using the Wilcoxon Rank-Sum test for non-normally distributed datasets that displayed equal variance, as determined using Lilliefors tests and Levene's tests respectively (Hollander et al., 2015). For normally distributed datasets with equal variance, as determined using Lilliefors tests and Bartlett's tests respectively (Hollander et al., 2015), we used one-way Analysis of Variance (ANOVA) and Student's t-tests to test for significant difference(s) in the mean values of key variables of weathered samples and their baseline counterparts. We tested for statistical significance between baseline groups and the broad groupings of lithology, experimental setting, stress conditions and pre-treatment type, rather than sub-sets of the groupings. Our statistical tests are supplemented by semi-quantitative, graphical displays of differences in sample strength relative to baseline conditions.

Results

Baseline siltstone characterisation

We recorded a mean Equotip *L*-value of 397.5 ± 126.7. The mean UCS was 34.15 MPa ± 6.43 MPa (Table 2). Failure occurred at a mean net strain of 1.47% ± 0.07% and mean local strain of 0.46% ± 0.21% (Figure 5). We calculated a mean Young's Modulus of 8.99 GPa ± 3.2 GPa. Most samples (n =10) displayed one or two stages of brittle failure before residual or zero strength was reached. For the modified geometry (*G)* samples, we observed mean UCS vales of 33.69 MPa ±1.57 MPa.

We undertook linear regression analysis of UCS as a function of pre-test bulk density and found a reasonably-strong, statistically-significant relationship (r^2 = 0.61, p = 0.003; Figure 6). The regression model envelope (Figure 6) allowed us to determine the representative baseline mean from which to compare the effect of weathering in absolute and percentage terms. If the initial starting bulk density of the post-test/weathered siltstone samples was less than or greater than the range of bulk density values measured in the baseline tests, they were not used in subsequent comparisons to weathered samples. This permitted more direct comparison of the effects of weathering on UCS and ensured the rock samples had comparable physical and geotechnical properties at the start of the experiments.

Siltstone visual appearance and surface hardness

The visual appearance of all samples changed during laboratory weathering experiments (Figure 7). We observed iron leaching, grain loss and slaking events Iron leaching was present for all stressed samples and in four control samples. Slaking (Figure 7 a, b) was characterised by loss of fragments of rock (typical long axis of 5 mm, typical short axis of 2 mm and 2 mm thick) (Figure 7 b). These fragments could be identified several weeks prior to detachment, characterised by sub-vertical cracks with a 1 to 2 mm aperture (Figure 7 b). We also observed tight (< 2 mm aperture), stepped, sub-horizontal cracks up to 50 mm long (Figure 7 c). All field samples displayed surface grain loss that resulted in a ‘powdery’ surface texture (Figure 7 d). Field samples also developed tight (< 2 mm aperture), stepped sub-horizontal cracks (2 to 10 mm in length) and tight, sub-vertical cracks (5 to 20 mm in length) (Figure 7 b, d). We did not observe any consistent relationships between

observed changes in the nature of weathering effects on surface texture and pre-treatment type (*U*, *P*, *G* or *PG*) and/or ambient compressive stress conditions (stressed vs. control) samples. All laboratory samples displayed a positive change in mass, with a mean of 5% ± 2.27%, while the field samples displayed a mean negative change in mass of -2.11% ± 3.08%. Of the field samples, we measured a positive change in mass for only three of the 16 samples.

For the laboratory experiments we assessed the relationship between surface hardness and week number (and, hence, time) using Pearson correlation. We did not observe a strong or statistically-significant relationship between these variables for both control (r = -0.21, p = 0.08) and stressed (r = -0.18, p = 0.14) samples. However, for the field experiments we observed a statistically-significant increase in surface hardness in both control (r = 0.21, p = 0.04) and stressed (r = 0.22, p = 0.03) samples.

General changes in siltstone compressive strength and strain values

Following completion of laboratory weathering experiments, control siltstone samples (all pre-treatment types) displayed a mean UCS of 16.72 MPa ± 1.64 MPa and failed at 1.15% ± 0.13% and 0.38% ±0.17% net and local strain, respectively (Table 3). We observed a mean Young's Modulus of 3.41 GPa ± 1.73 GPa. Stressed siltstone samples (all pre-treatment types) displayed a mean UCS of 18.89 MPa ± 3.95 MPa, failing at 1.19% ± 0.16% and 0.27% ± 0.18% net and local strain respectively. We observed a mean Young's Modulus of 1.69 GPa ± 0.03 GPa (Table 3). Normalised stress-strain curves for laboratory experiments relative to baseline tests are displayed in Figure 8 a. Stressed *U*-type samples displayed a single stage of brittle

failure, while all other samples displayed at least two stages of brittle failure. (Table 3).

For field weathering experiments, control siltstone samples (all pre-treatment types) displayed a mean UCS value of 36.71 MPa ± 14.93 MPa, failing at 1.4% ± 0.09% and 0.26% ± 0.17% net and local strain respectively. We observed a mean Young's Modulus value of 5.0 GPa ± 1.52 GPa (Table 4). Stressed siltstone samples (all pre-treatment types) displayed a UCS value of 37.30 MPa ± 13.74 MPa, failing at 1.12% ± 0.1% and 0.29% ± 0.17% net and local strain respectively. We observed a mean Young's Modulus value of 3.63 GPa ± 2.79 GPa, (Table 4). Normalised stress-strain curves relative to baseline tests are displayed in Figure 8 b. Stressed *P*-type samples displayed a single stage of brittle failure, while all other samples displayed at least two stages of brittle failure. (Table 4).

Siltstone: Experimental setting

For siltstone samples weathered under laboratory conditions we observed a mean UCS of 17.81 MPa ± 3.10 MPa, equivalent to an absolute reduction in mean UCS of 12.70 MPa, or 41.36% ($p < 0.001$) (Table 5). We recorded a reduction in mean net strain at failure of 20.69% ($p < 0.001$), and mean reduction in Young's Modulus of 69.7% ($p = 0.001$). These changes in mean conditions are also indicated in Figure 9 a & b, which demonstrates a shift in the kernel density estimates of normalised axial stress and strain to values lower than those observed in baseline tests. For siltstone samples weathered in field conditions, we observed a mean UCS of 37.10 MPa ± 13.57 MPa, which is not statistically-significantly different from baseline values ($p = 0.583$; Figure 9 b). Strain at failure values decreased ($p > 0.001$) relative to those

observed in baseline tests (12.55%), but overall variability increased (Figure 9 b). with Young's Modulus values also decreasing by 54.54% (p =0.006).

Siltstone: Effect of ambient compressive stress

Siltstone control samples displayed a mean UCS of 25.81 MPa ± 14.13 MPa, equivalent to an absolute reduction in mean UCS of 6.34 MPa, or 22.26% (p = 0.043) (Table 5). We recorded a reduction in mean net strain at failure and Young's Modulus of 14.31% (p > 0.001) and 54.96% (p = 0.0065), respectively. Figure 9 c & d demonstrates a shift in the kernel density estimates of normalised axial stress and strain to values lower than those observed in baseline tests, with overall variability in normalised axial stress (UCS) increased (Table 5). For stressed siltstone samples, we observed a mean UCS of 28.80 MPa ± 13.86 MPa, equivalent to a reduction of 4.3 MPa, or 14.52% (p = 0.043; Figure 9 c). Strain-at-failure values decreased (p = 0.002) relative to those observed in baseline tests (18.57 %) (Figure 9 d), as did Young's Modulus (p = 0.001, 66.82%) (Table 5). No statistically-significant differences exist between the mean UCS, strain-at-failure, and Young's Modulus values of stressed and control siltstone samples (p = 0.262, p = 0.044, and p = 0.300, respectively) (Figure 9 c).

Vertical strain measurements recorded during the weathering experiments indicated that each of the 8 stressed samples in the laboratory experiments compressed over the duration of the laboratory weathering test. We observed small-scale expansion events (-0.01 % to -0.02 % strain) on time-scales greater than that of the wetting and drying cycles that lasted for week long periods. We also observed elastic rebound of the samples at the end of the tests when the load was removed. *U* and *P* samples

displayed no permanent strain over the course of the experiment, in contrast to the *G and PG* samples, which displayed permanent strain values of 0.01 % to 0.16 % at the end of the weathering experiment.

Siltstone: Effect of pre-treatment type

For *U*- and *P*--type samples, mean UCS values were statistically-significantly (p = 0.001 and p = 0.042, respectively) lower than those observed in baseline tests; we recorded reductions in mean UCS of 38.28% and 20.28% respectively (Table 5; Figure 9 e). *G*- and *PG*-type samples did not show statistically-significant changes (p = 0.159 and p = 0.116 respectively) in mean UCS values relative to those observed in baseline tests. Siltstone sample modifications displayed lower kernel density distributions for strain-at-failure values relative to baseline ($p < 0.022$) (Figure 9 f). Young's Modulus values were all lower than those observed in baseline tests, indicating a decrease in sample stiffness ($p < 0.05$) (Table 5).

Baseline sandstone characterisation

We recorded a mean Equotip *L*- value of 564.87 ± 68.73. The mean UCS was 55.69 MPa ± 7.61 MPa (Table 2). Failure occurred at a mean net strain of 1.25% ± 0.07% and mean local strain of 0.24% ± 0.14%. We calculated a mean Young's Modulus of 5.69 GPa ± 0.86 GPa. All baseline sandstone samples exhibited a single-stage brittle failure (Figure 5). For the modified geometry (*G*) samples, we observed mean UCS values of 48.75 MPa ± 3.2 MPa. We did not observe a strong or statistically-significant relationship between UCS and bulk density for the sandstone samples (r^2 = 0.1626, p = 0.2188). To consider the effects of weathering on the strength of

sandstone, we therefore compared absolute and percent changes in UCS for weathered samples to the overall baseline mean value.

Sandstone visual appearance and surface hardness

The visual appearance of all samples changed during laboratory weathering experiments, principally by surficial grain loss, with occasional sub-horizontal cracking. Iron leaching was evident for all stressed laboratory samples (Figure 7 e). Surficial grain loss was observed in all field samples; this occurred in concentrated 'pockets' for three samples (Figure 7 f), though there was no relationship with pre-treatment type of ambient stress conditions. We did not observe surface cracking or slaking in control or stressed samples for both laboratory or field experiments. We measured a positive change in mass for all laboratory samples, with a mean of 1.72% ± 0.72%. We measured a positive change in mass for 10 field samples, with the remaining 6 samples displaying a negative change in mass. As such, field samples displayed a mean change in mass of -0.62% ± 3.32%. For laboratory samples we observed a statistically-significant net decrease in surface hardness through time for both control (r = -0.26, p = 0.023) and stressed (r = -0.36, p = 0.001) samples. For field samples we observed a statistically-significant increase in surface hardness in both control (r = 0.4, p < 0.001) and stressed (r = 0.44, p < 0.001) samples.

General changes in Sandstone compressive strength and strain values

Following completion of laboratory weathering experiments, control sandstone samples displayed a mean UCS of 35.76 MPa ± 7.5 MPa and failed 1.23% ± 0.09%

and 0.22% ± 0.2% net and local strain, respectively (Table 3). We observed a mean Young's Modulus of 6.58 GPa ± 1.47 GPa (Table 3). Stressed sandstone samples (all pre-treatment types) displayed a mean UCS value of 38.73 MPa ± 7.32 MPa, failing at 1.25% ± 0.09% and 0.27% ± 0.16% net and local strain, respectively. Normalised stress-strain curves relative to baseline tests are displayed in Figure 8 c. We observed a mean Young's Modulus value of 5.49 GPa ± 0.38 GPa (Table 3). All samples displayed at least two stages of brittle failure (Table 3).

For field weathering experiments, control sandstone samples displayed a mean UCS value of 49.93 MPa ± 7.84 MPa and failed at 1.23% ± 0.19% and 0.22% ± 0.16% net and local strain, respectively (Table 4). Normalised stress-strain curves relative to baseline tests are displayed in Figure 8 d. We observed a mean Young's Modulus value of 7.07 GPa ± 2.39 GPa (Table 4). All field control sandstone samples displayed two stages of brittle failure (Table 4). Field stressed sandstone samples displayed a mean UCS value of 44.53 MPa ± 14.16 MPa and failed at 1.23% ± 0.19% and 0.17% ± 0.14% net and local strain, respectively. We observed a mean Young's Modulus value of 6.90 GPa ± 0.86 GPa (Table 4). Stressed *PG*-type samples displayed a single stage of brittle failure. *U- and G*-type samples displayed two stages of brittle failure. *P*-type samples displayed three stages of brittle failure (Table 4).

Sandstone: Experimental setting

For sandstone samples weathered under laboratory conditions, we observed a mean UCS of 37.24 MPa ± 7.32 MPa, equivalent to an absolute reduction in mean UCS of 18.45 MPa, or 33.12% (Table 5). This overall reduction in UCS ($p < 0.001$) relative to

those observed in baseline tests is statistically significant (Figure 10 a). We recorded a reduction in mean net strain at failure of 0.38% and an increase in mean Young's Modulus of 6.06%, which were not statistically significantly (p = 0.884 and p = 0.460, respectively) different from baseline tests (Figure 10 b) (Table 5).

For sandstone samples weathered in field conditions, we observed a mean UCS of 47.23 MPa ± 11.40 MPa, which is statistically-significantly lower (8.46 MPa, or 15.19%) than baseline values (p = 0.042) (Figure 10 a). We recorded a reduction in mean net strain at failure of 1.81%, which was not statistically significant (p = 0.632) from baseline tests (Figure 10 b), along with a statistically significant increase in mean Young's Modulus of 22.8% (p = 0.04) (Table 5).

Sandstone: Effect of ambient compressive stress

Sandstone control samples displayed a mean UCS of 42.85 MPa ± 10.41 MPa, equivalent to an absolute reduction in mean UCS of 12.84 MPa, or 23.06% (Table 5). This statistically-significant change in mean UCS (p = 0.043 and p = 0.001) is also evident in Figure 10 c. We recorded a reduction in mean net strain at failure of 1.53% and an increase in mean Young's Modulus of 19.98%, which were not statistically-significantly different (p = 0.538 and p = 0.089, respectively) from baseline tests (Figure 10 d) (Table 5). For sandstone stressed samples we observed a mean UCS of 41.63 MPa ± 11.29 MPa, which is statistically-significantly lower (14.06 MPa, or 25.25%) than baseline values (p = 0.042) (Figure 10 c). We recorded a reduction in mean net strain at failure of 0.66 % and an increase in mean Young's Modulus of 8.88%, which were not statistically-significantly different (p = 0.847 and p = 0.250, respectively) from baseline tests (Figure 10 d) (Table 5). No statistically-

significant differences exist between the mean UCS, strain-at-failure values, and Young's Modulus of stressed and control sandstone samples (p = 0.006, p = 0.668, and p = 0.204, respectively) (Figure 10 c).

The same behaviour as seen for the monitored strain measurements for stressed siltstone samples is observed for the stressed sandstone samples, with six samples compressing in the direction of load over test duration. We observed expansion events on the order of days to weeks, which exerted –0.025 % to -0.1 % strain (Figure 11). We recorded rebound of samples at the end of the tests when the load was removed, with *U* and *P* displaying no permanent strain while *G* and *PG* samples displayed permanent strain values of 0.01% to 0.05% strain.

Sandstone: Effect of pre-treatment type

For *U*-, *P*- and *G*--type samples, mean UCS values were statistically-significantly (p < 0.001, p = 0.008 and p = 0.008, respectively) lower than those observed in baseline tests; we recorded mean reductions in UCS of 13.69%, 12.77% and 11.58%, respectively (Table 5; Figure 10 e). *PG*-type samples did not show statistically-significant changes (p = 0.089) in mean UCS values relative to those observed in baseline tests. Sandstone sample modifications displayed a similar distribution in strain-at-failure values to baseline (Figure 10 f), with no statistically-significant changes observed. Young's Modulus values were all higher than those observed in baseline tests, indicating an increase in sample stiffness (Table 5). For *U* samples this increase was statistically significant (p = 0.023*)*.

Failure mode

For both siltstone and sandstone samples tests, single-stage failures occurred in samples that displayed the highest UCS values. As UCS sample strength decreased, failure mode changed to include more brittle stages of failure or 'stress-drops' before residual strength was achieved. Both lithologies displayed this behaviour (Figure 12), with significant differences in strength for each failure style existing for sandstone ($p < 0.010$; Figure 12b). These multi-stage failures may often sustain stresses slightly lower (~1 MPa to 2 MPa) than peak strength of the sample until further or final failure occurs (Figure 12c). Along with changes in stress-strain behaviour, a greater number of cracks and associated complexity of failure morphology were observed within the samples with increasing number of brittle failure stages (Figure 12d). No correlations existed between failure mode and environmental setting, test conditions or sample pre-treatments.

Discussion

Controls on visual appearance and surface hardness

Our weathering experiments were designed to understand controls on weathering intensity, including the influence of ambient compressive stress, stress history and local stress concentrations. Our monitoring during the experiments revealed that changes in the visual appearance of samples and surface hardness showed little sensitivity to pre-treatment. We note surface textures and degradation processes that are common to both lithologies, notably surficial grain loss, iron leaching and surface cracking. However, we also observed consistent patterns in surface texture that highlight the importance of lithology and the mechanism of weathering as acting as a control on the type and nature of surface appearance and texture. For example,

siltstone samples experienced slaking events in response to laboratory saltwater submergence and exposure cycles, as is commonly observed in argillaceous lithologies (Qi et al., 2015). In contrast, slaking was not observed in the field tests on siltstone; in this weathering environment where full saltwater submergence did not occur and where wetting resulted from precipitation, samples weathered by surficial grain loss that resulted in a distinctive 'powdery' surface texture. Critically, the pre-treatment type and/or ambient compressive stress condition did not affect the surficial weathering processes operating in the siltstone samples. For the sandstone samples, there was no obvious difference in the mechanism of weathering and the resultant surface response between laboratory and field tests; grain loss and cracking dominated in both settings. However, the presence of an ambient compressive stress resulted in more pronounced iron leaching, possibly due to sample dilatancy and permeability in response to stress application (Mitchell and Faulkner, 2009; Nicholson, 2001; Oda et al., 2002; Zoback and Byerlee, 1975). In turn, this likely facilitated oxidation, solution and water-borne removal of iron present in the sandstone samples.

The controls of lithology and mechanism of weathering were also manifest in the nature of changes in the surface hardness of samples throughout the weathering experiments. Siltstone samples weathered in the laboratory did not show any change in surface hardness. In contrast, siltstone samples weathered in field conditions showed an increase in surface hardness. Sandstone samples weathered in the laboratory displayed a reduction in surface hardness, possibly resulting from a more dispersed loss of grains and a loss of near-surface cement. In contrast, field samples displayed an increase in surface hardness, in part due to the less-widely distributed

grain loss in isolated ‘pockets’, permitting case hardening to develop in areas not experiencing concentrated grain loss (Mol and Viles, 2012; Viles et al., 2011). Biogenic case hardening may also explain the increase in surface hardness for field samples, while the saline brine of the laboratory experiments prevented the development of such a crust (Slavík et al., 2017).

Controls on weathering induced strength degradation

Our geotechnical analysis indicates that pre-existing micro-crack damage, modified sample geometries and/or samples subjected to a constant compressive vertical stress do not result in enhanced strength degradation relative to samples that have undergone no modification. We note that not all reductions in mean values of UCS were statistically-significant in some pre-treatment groups, but we observed decreases in the modal value(s) of UCS occurring in all samples, indicative of a general trend (Figures 9 and 10).

A greater density of initial micro-cracks, as present in *P* samples, does not necessarily result in a greater degree of strength reduction, resulting from exploitation of micro-crack populations by weathering processes. This is in contrast to other studies, where increased surface area as a result of micro-cracking, or pre-existing damage within a sample due other weathering processes have been observed to accelerate the rate of weathering (Røyne et al., 2008, Viles et al., 2018). The removal of the high compressive stresses used in the pre-damaging process prior to commencing the weathering experiments may have permitted any newly-created microcracks to contract. High, damaging stresses may need to be maintained during operation of weathering processes for intergranular flaws to be

exploited and a more obvious control on strength reduction to be observed. We suggest that the nature of stress history and if and how this stress is maintained may be important. The degree of geometric modification in *P* and *PG* sample may have been insufficient to create stress concentrations of sufficient magnitude to result in enhanced micro-cracking (Lajtai and Lajtai, 1974). We suggest that differing cliff-face surface geometries at a range of scales may significantly generate greater stress concentrations that can be preferentially weathered than created by our sample modifications (Martel, 2006; Brain et al., 2014).

However, within this experimental set-up and over the time-scale of the experiments considered, a constant compressive stress has a negligible effect on strength degradation resulting from weathering processes, with no statistically significant differences between the UCS values of control and stressed samples for both lithologies. This indicates that the ambient stress environment does not affect the intensity of weathering and its effect on compressive strength within the ambient stress range and experimental set-up considered here.

This result is in contrast to experiments conducted using sediments with no cementation (Bruthans et al., 2014; Zhang et al., 2015) or weak cementation (Bruthans et al., 2016; Rihosek et al., 2016). These previously-published experiments showed a temporal component of stress influence on weakening, displaying faster erosion rates (Bruthans et al., 2014) and strength degradation (Zhang et al., 2015) until a 'critical' stress value was reached. The interlocking strength of the grains was great enough to slow or prevent further erosion and weathering from occurring. The frictional properties of these materials were the

dominant components of strength, rather than cohesional properties of intact rock. Martin and Chandler (1994) proposed that the strength of intact rock is controlled primarily by cohesion up until 75% to 80% of UCS. Our findings suggest that gravitationally-induced compressive stress (here 2 MPa and 3.8 MPa) has a limited impact on the processes which result in cohesional strength reduction. This imposed topographic stress may also be of an insufficient magnitude when combined with stresses generated by weathering to cause any volumetric changes via contraction or dilation of cracks in the rock samples that could subsequently be exploited by weathering processes. This is despite the enhanced leaching observed, and greater permeability postulated, in stressed sandstone samples. Higher ambient stresses that cause crack initiation (σ_{ci}) and/or propagation (σ_{cd}) may cause weathering and sub-critical crack growth processes to drive greater differences in compressive strength between control and stressed samples. The significance of the magnitude of the ambient stress environment has been observed in laboratory tests where ambient stress environments are tensile (Voigtländer et al., 2018).

Effect of weathering on compressive rock strength

Overall, we demonstrate that weathering results in a significant reduction of strength for all laboratory samples and even for rock that has been exposed to natural environmental conditions for a year, as demonstrated by the 15.19% loss in strength for sandstone samples placed at the cliff-top. The observed reductions in intact rock strength are likely to result from a combination of factors, in addition to those that are evident in the observed surficial changes in the rock, such as slaking, cracking and grain loss. For example, sub-critical crack growth throughout the rock samples may

be a key driver, where micro-crack growth occurs at stresses lower than the crack initiation threshold within a rock mass (Atkinson, 1984). Small amplitude stress as a result of environmental processes such as insolation or wetting and drying can therefore drive micro-crack growth (Eppes and Keanini, 2017). This can occur via stress corrosion cracking where molecular bonds are strained and stretched at crack tips by a chemically active environmental agent, such as water (Atkinson, 1984; Eppes and Keanini, 2017; Voigtländer et al., 2018). This process is enhanced where chemical conditions are conducive to corrosion; changes in the geochemistry, as evidenced by leaching, may subsequently change sub-critical cracking characteristics, though little is known about the exact controls on this process (Atkinson, 1984; Dunning and Huf, 1983; Freiman, 1984).

We noted a greater reduction in UCS in both lithologies for samples weathered under laboratory conditions, highlighting the importance of weathering process in driving degradation of rock strength. In particular, we note the relative efficacy of salt as a weathering agent and in driving strength loss of intact rocks (cf. Goudie et al., 1970). We observed significant periods of expansion within the laboratory strain data, indicating that such expansion was able to counteract the 3.8 MPa vertical stress acting on the sample. This potentially explains the limited influence of topographic stress on strength as weathering can generate stresses that counteract those generated by overburden loading.

We observed a mismatch between the two measures of strength that we used. Notably, the reductions in UCS recorded following the completion of weathering experiments were not evident in any statistically-significant trends in surface

hardness during the experiment in all samples. In field-weathering sandstone samples, surface hardness increased, despite a decrease in ultimate UCS. This inconsistency indicates that our interpretation of rock strength from visual observations and surface hardness data may not capture the 'internal' weakening of intact rock. This internal weakening is of critical importance to shallow rock slope failures, where release of an incipient failure mass is contingent on brittle fracture through intact rock (Collins and Stock, 2016). Our results indicate that use of surface hardness measurements in constraining the influence of weathering on intact rock strength and, hence, shallow rock slope failure that show visible evidence of weathering may be limited and/or not appropriate in all situations (see Aoki and Matsukura, 2007; Coombes et al., 2013; Viles et al., 2011).

Effects of weathering on failure style

Our results suggest that the two lithologies display differing responses to weathering in terms changes to strain-at-failure values. We observed no change in strain-at-failure values in weathered sandstone samples when compared to baseline tests. In contrast, siltstone samples displayed statistically-significant reductions in strain-at-failure values relative to baseline values. Weathered siltstone samples also displayed mean Young's modulus values that are statistically-significantly lower than baseline values. An explanation of these differences in strain and elasticity between lithologies is enigmatic but may result from a greater degree of softening and ductility in the siltstone samples due to the presence of clay minerals (Fabre and Pellet, 2006). The siltstone may be more susceptible to granular rearrangement than the

highly-cemented sandstone, which undergoes considerably less plastic deformation at values less than UCS.

Our analysis indicates that a reduction in strength is linked to and manifest in a change in failure style. Weaker rocks display a more distributed multi-stage failure process reflected in their stress-strain behaviour and the resultant failure morphology (as observed also in studies by Basu et al., 2009; Gupta and Seshagiri Rao, 2000). Multi-stage failures involve several stages of macro-scale fracture and strength loss until residual or total loss of strength occurs. These types of failure can temporally sustain high stress levels even after a peak stress level has been reached. It is only after sufficient post-peak strain has accumulated within the sample that subsequent failure event(s) occur. Weakening of the rock sample by weathering may lead to more diffuse micro-cracking that eventually results in an increased number of macro-cracks, as seen in cyclic loading tests, which can be used as a proxy for environmental fluctuations and associated weathering processes (Cerfontaine and Collin, 2017). These distributed micro-cracks do not result in the same pattern of coalescence required for unstable 'run-away' macro-scale fracture, as normally predicted for a similar point on stress-strain curves (Eberhardt et al., 1998; Martin and Chandler, 1994). The failure events observed in the multi-failure stage failures instead may represent mini-coalescence events in weaker zones to form relatively smaller macro-scale fractures, which do not connect in the first instance.

Implications for shallow rock slope failures

We suggest that a change in failure style and strength loss over time (Figure 13) will determine the nature of triggers required for failure to occur and will hence dictate

the timing of ultimate failure. Intact rock characterised by single-stage brittle fracture likely requires a higher magnitude loading event that will result in near-instantaneous failure, as indicated in Figure 13. Two-stage brittle failure likely still require a relatively higher magnitude loading event for an initial fracture event to occur and may require another similar magnitude loading event for final failure to occur (Figure 13). The timing between two such events may be potentially be prolonged, resulting in a quasi-stable state (Leroueil, 2001). As damage accumulates through time, the magnitude of environmental stresses required for fracture to occur decreases (Figure 13), but the frequency of such events will likely increase, resulting in a positive feedback and potential pattern of acceleration towards ultimate failure. Figure 14 illustrates this process, with each 'new' failure event weakening the rock, so that the next stage of brittle fracturing requires a lower magnitude of stress to act as a trigger for further failure. This multi-stage failure processes may be represented as 'step-wise' fracture through multiple rock bridges or partial fracturing through an individual rock bridge, where fracture represents an initial failure stage of the stress–strain graph (Brideau et al., 2009; Eberhardt et al., 2004b; de Vilder et al., 2017). For final failure to occur, only a low magnitude stress perturbation may be required (Figure 14) due to the critical concentration of micro-cracks and accumulated damage within the rock (Main, 2000). In the context of rock slope failure, this final stress perturbation may reflect stress-redistribution of the slope following progressive failure (e.g. Eberhardt et al., 2004a; Rosser et al., 2007; Stock et al., 2012), environmental stress fluctuations (Collins and Stock, 2016; Gischig et al., 2011; Gunzburger et al., 2005; Moore et al., 2011) or topographic stress concentrations within the slope (Brain et al., 2014). In such a scenario, even though topographic stress is not a

control on the rate of weakening, as we have determined from our experimental datasets, it may therefore control the location of rock failure.

As final failure occurs a distinct period of time after the initial damaging loading event (such as an earthquake or storm), this may explain the low observed correlations between environmental variables and failure (Lim et al., 2010; Rosser et al., 2007; Stock et al., 2012), with a 'lag' between initial and final failure. Monitoring observations have revealed that external precipitation triggering events can initiate extended periods of increased and accelerated deformation indicating a critical damage threshold has been reached in the rock, with previous observations showing that in some settings that this can accelerate to final failure within a week (Carlà et al., 2018; Kromer et al., 2017a; Loew et al., 2016). Observations of pre-failure deformation that did not result in a hyperbolic acceleration towards failure may represent a failure sequence where a significant 'lag' effect exists between the initial and final failure events (Carlà et al., 2018). Such a 'lag' effect suggests that weathered rock slopes may adjust more slowly to changing environmental conditions.

This multi-stage and prolonged failure sequence may also be reflected in the resulting failure scar surface, where greater roughness coupled with surficial weathering provide an indication of failure history. Weathered and broken rock bridges can represent an initial failure event, which has been followed by a sufficiently long period for substantial surficial weathering (i.e. damage accumulation in Figure 14) to occur before the final loss of strength and collapse (de Vilder et al., 2017). In addition, the greater strain that can be sustained in the weathered samples

increases, suggesting that weathered rock bridges can sustain greater levels of strain before final detachment occurs. This may have important implications for monitoring of pre-failure deformation; our results suggest that a universal value of 'critical strain' is unlikely to be valid for a given rock type and will depend on the degree of weathering experienced by any individual section of rockslope. Pre-failure deformation may also record several stages of macro-scale brittle failure related to rock bridge fracture (Figure 14)(Carlà et al., 2017; Kromer et al., 2015; Royan et al., 2015). The change in failure style may dictate the degree of discernible pre-failure deformation, with multi-failure events potentially displaying higher degrees of pre-failure deformation than compared to single stage events as the period of time over which total loss of strength occurs is longer (Kromer et al., 2017b; Petley et al., 2005; Williams et al., 2018). The time-scales over which such deformation could be observed is also dependent on the exact rock bridge attributes within an incipient failure mass, with the amount of deformation increasing for larger rockfalls (Kromer et al., 2017b), reflecting the breakage of multiple rock bridges (de Vilder et al., 2017). We, therefore, hypothesise that as a rock slope weakens through time, the mechanics of rockfall detachment are likely to change.

Conclusion

We conducted a series of experiments on coarse- and fine-grained sedimentary rocks under constant uniaxial compressive stress to constrain the relationship between exposure to various environmental conditions, compressive stress and ultimate failure behaviour. We modified samples to account for pre-existing micro-crack damage within the rock, as well as increased surface area and localised stress

concentrations created by slope geometry. Our experimental dataset reveals that weathering does result in a reduction in unconfined compressive strength, though the applied compressive stresses of 2 and 3.8 MPa neither enhance nor dampen the degree of weathering-induced strength loss. In isolation, this result suggests that sections of rock slope subjected to high stresses will not preferentially weaken in response to weathering relative to sections under no ambient stress. However, we suggest that our findings may be specific to the lithologies considered here, where cohesional strength dominates over friction. In addition, greater ambient stresses as a proportion of ultimate strength may be possible in certain topographic settings, influencing mechanisms of weathering. Alongside this, pre-existing damage and increased surface roughness also have no discernible influence on the magnitude of strength reduction resulting from weathering. The reduction in UCS strength is not consistently reflected in a reduction of surface hardness, placing limits on the interpretation of intact rock strength made solely based on surface hardness monitoring.

In our experiments, weathering resulted in considerable changes in the style of failure, even over relatively short (three months to one year) timescales. Weathered weaker samples developed post-peak strength and so several stages of macro-scale fracture were required before a total loss of strength was observed. We suggest that these multiple fracture events may be representative of complete or partial rock bridge fracture. As post peak strength evolves, we theorise that the magnitude of triggering events that result in brittle facture, and ultimately rockfall release, decreases. This provides further explanation of rockfall activity that occurs in response low-magnitude environmental forcing that are conventionally considered to

be too low to cause shallow rock slope failure. The associated prolonged sequence of brittle fracture may be manifested in step-wise patterns of pre-failure deformation data. Weathering induced strength degradation, therefore, may alter the rock slope response to environmental loading events and the subsequent mechanical evolution of failure.

References

Aldred J, Eppes MC, Aquino K, Deal R, Garbini J, Swami S, Tuttle A, Xanthos G. 2016. The influence of solar-induced thermal stresses on the mechanical weathering of rocks in humid mid-latitudes. Earth Surface Processes and Landforms **41** : 603–614. DOI: 10.1002/esp.3849

Aoki H, Matsukura Y. 2007. A new technique for non-destructive field measurement of rock-surface strength: an application of the Equotip hardness tester to weathering studies. Earth Surface Processes and Landforms **32** : 1759–1769. DOI: 10.1002/esp.1492

ASTM D7012-14. 2014. Standard test methods for compressive strength and elastic moduli of intact rock core specimens under varying states of stress and temperature . ASTM International: West Conshohocken, PA

Atkinson BK. 1984. Subcritical crack growth in geological materials. Journal of Geophysical Research **89** : 4077–4114. DOI: 10.1029/JB089iB06p04077

Bachmann D, Bouissou S, Chemenda A. 2004. Influence of weathering and pre-existing large scale fractures on gravitational slope failure: insights from 3-D physical modelling. Natural Hazards and Earth System Science **4** : 711–717. DOI: 10.5194/nhess-4-711-2004

Barla G, Barla M, Debernardi D. 2010. New triaxial apparatus for rocks. Rock Mechanics and Rock Engineering **43** : 225–230. DOI: 10.1007/s00603-009-0076-7

Basu A, Celestino TB, Bortolucci AA. 2009. Evaluation of rock mechanical behaviors under uniaxial compression with reference to assessed weathering grades. Rock Mechanics and Rock Engineering **42** : 73–93. DOI: 10.1007/s00603-008-0170-2

Brain MJ, Rosser NJ, Norman EC, Petley DN. 2014. Are microseismic ground displacements a significant geomorphic agent? Geomorphology **207** : 161–173. DOI: 10.1016/j.geomorph.2013.11.002

Brideau M, Yan M, Stead D. 2009. The role of tectonic damage and brittle rock fracture in the development of large rock slope failures. Geomorphology **103** : 30–49. DOI: 10.1016/j.geomorph.2008.04.010

Bruthans J, Filippi M, Schweigstillová J, Řihošek J. 2016. Quantitative study of a rapidly weathering overhang developed in an artificially wetted sandstone cliff. Earth Surface Processes and Landforms **723** : 711–723. DOI: 10.1002/esp.4016

Bruthans J, Soukup J, Vaculikova J, Filippi M, Schweigstillova J, Mayo AL, Masin D, Kletetschka G, Rihosek J. 2014. Sandstone landforms shaped by negative feedback between stress and erosion. Nature Geoscience **7** : 597–601.

Carlà T, Farina P, Intrieri E, Botsialas K, Casagli N. 2017. On the monitoring and early-warning of brittle slope failures in hard rock masses: Examples from an open-pit mine. Engineering Geology **228** : 71–81. DOI: 10.1016/j.enggeo.2017.08.007

Carlà T, Farina P, Intrieri E, Ketizmen H, Casagli N. 2018. Integration of ground-based radar and satellite InSAR data for the analysis of an unexpected slope failure in an open-pit mine. Engineering Geology **235** : 39–52. DOI: 10.1016/j.enggeo.2018.01.021

Cerfontaine B, Collin F. 2017. Cyclic and Fatigue Behaviour of Rock Materials: Review, Interpretation and Research Perspectives. Rock Mechanics and Rock Engineering **51** : 1–24. DOI: 10.1007/s00603-017-1337-5

Clarke BA, Burbank DW. 2010. Bedrock fracturing, threshold hillslopes, and limits to the magnitude of bedrock landslides. Earth and Planetary Science Letters **297** : 577–586. DOI: 10.1016/j.epsl.2010.07.011

Collins BD, Stock GM. 2016. Rockfall triggering by cyclic thermal stressing of exfoliation fractures. Nature Geoscience **9** : 395–400. DOI: 10.1038/NGEO2686

Coombes MA, Feal-Pérez A, Naylor LA, Wilhelm K. 2013. A non-destructive tool for detecting changes in the hardness of engineering materials: Application of the Equotip durometer in the coastal zone. Engineering Geology **167** : 14–19. DOI: 10.1016/j.enggeo.2013.10.003

Dunning JD, Huf WL. 1983. The effects of aqueous chemical environments on crack and hydraulic fracture propagation and morphologies. Journal of Geophysical Research **88** : 6491–6499.

Durgin PB. 1977. Landslides and the weathering of granitic rocks. Geological Society of America **3** : 127–131.

Dussauge-Peisser C, Helmstetter A, Grasso JR, Hantz D, Desvarreux P, Jeannin M, Giraud A. 2002. Probabilistic approach to rock fall hazard assessment: potential of historical data analysis. Natural Hazards and Earth System Sciences **2** : 15–26. DOI: 10.5194/nhess-2-15-2002

Eberhardt E, Stead D, Coggan JS. 2004a. Numerical analysis of initiation and progressive failure in natural rock slopes—the 1991 Randa rockslide. International Journal of Rock Mechanics and Mining Sciences **41** : 69–87. DOI: 10.1016/S1365-1609(03)00076-5

Eberhardt E, Stead D, Coggan JSS. 2004b. Numerical analysis of initiation and progressive failure in natural rock slopes—the 1991 Randa rockslide. International Journal of Rock Mechanics and Mining Sciences **41** : 69–87. DOI: 10.1016/S1365-1609(03)00076-5

Eberhardt E, Stead D, Stimpson B, Read RS. 1998. Identifying crack initiation and propagation thresholds in brittle rock. Canadian Geotechnical Journal **35** : 222–233.

Eberhardt E, Stimpson B, Stead D. 1999. Effects of grain size on the initiation and propagation thresholds of stress-induced brittle fractures. Rock Mechanics and Rock Engineering **32** : 81–99.

Einstein HH, Veneziano D, Baecher GB, O'Reilly KJ, Reilly JO. 1983. The effect of

discontinuity persistence on rock slope stability. International Journal of Rock Mechanics and Mining Sciences **20** : 227–236. DOI: 10.1016/0148-9062(83)90003-7

Eppes M-C, Keanini R. 2017. Mechanical Weathering and Rock Erosion by Climate-Dependent Subcritical Cracking. Reviews of Geophysics **55** : 1–39. DOI: 10.1002/2017RG000557

Eppes MC, Magi B, Hallet B, Delmelle E, Mackenzie-Helnwein P, Warren K, Swami S. 2016. Deciphering the role of solar-induced thermal stresses in rock weathering. Geological Society of America Bulletin **128** : 1315–1338. DOI: 10.1130/B31422.1

Fell R, Corominas J, Bonnard C, Cascini L, Leroi E, Savage WZ. 2008. Guidelines for landslide susceptibility, hazard and risk zoning for land-use planning. Engineering Geology **102** : 99–111. DOI: 10.1016/j.enggeo.2008.03.014 [online] Available from: http://dx.doi.org/10.1016/j.enggeo.2008.03.014

Fookes PG, Gourley CS, Ohikere C. 1988. Rock weathering in engineering time. Quarterly Journal of Engineering Geology **21** : 33–57.

Freiman SW. 1984. Effect of chemical enviroments on slow crack growth in glasses and ceramics. Journal of Geophysical Research **89** : 4072–4076.

Gischig VS, Moore JR, Evans K., Amann F, Loew S. 2011. Thermomechanical forcing of deep rock slope deformation : 1 . Conceptual study of a simplified slope. Journal of Geophysical Research **116** : 1–18. DOI: 10.1029/2011JF002006

Goodman RE, Shi G. 1985. Block Theory and its Application to Rock Engineering . Prentice-Hall Inc: New Jersey

Goudie A, Cooke R, Evans I. 1970. Experimental investigation of rock weathering by salts. Area **2** : 42–48.

Goudie AS. 2016. Quantification of rock control in geomorphology. Earth-Science Reviews **159** : 374–387. DOI: 10.1016/j.earscirev.2016.06.012

Gunzburger Y, Merrien-Soukatchoff V, Guglielmi Y. 2005. Influence of daily surface temperature flucuations on rock slope stability: a case study of the Rochers de Valabres slope (France). International Journal of Rock Mechanics and Mining Sciences **42** : 331–349.

Gupta AS, Seshagiri Rao K. 2000. Weathering effects on the strength and deformational behaviour of crystalline rocks under uniaxial compression state. Engineering Geology **56** : 257–274. DOI: 10.1016/S0013-7952(99)00090-3

Guzzetti F, Carrara A, Cardinali M, Reichenbach P. 1999. Landslide hazard evaluation: A review of current techniques and their application in a multi-scale study, Central Italy. Geomorphology **31** : 181–216. DOI: 10.1016/S0169-555X(99)00078-1

Head KHK, Epps RJ. 2011. Manual of Soil Laboratory Testing, Volume 2: Permeability, Shear Strength and Compressibility Tests . 3rd ed. Whittles Publishing:

Caithness

Hencher SRI, McNicholl DP. 1995. Engineering in weathered rock. Quarterly Journal of Engineering Geology **28** : 253–266.

Hollander M, Wolfe DA, Chicken E. 2015. Nonparametric Statistical Methods . 3rd ed. John Wiley & Sons

Huisman M, Nieuwenhuis JD, Hack HRGK. 2011. Numerical modelling of combined erosion and weathering of slopes in weak rock. Earth Surface Processes and Landforms **36** : 1705–1714. DOI: 10.1002/esp.2179

Iverson RM. 2000. Landslide triggering by rain infiltration. Water Resources Research **36** : 1897–1910. DOI: 10.1029/2000WR900090

Jaeger JC, Cook NGW, Zimmerman R. 2007. Fundamentals of Rock Mechanics . 4th ed. Wiley-Blackwell

Jennings JE. 1970. A mathematical theory for the calculation of the stability of open cast mines. 87–102 pp.

Keefer DK et al. 1987. Real-time landslide warning during heavy rainfall. Science **238** : 921–925.

Keefer DK. 1994. The importance of earthquake-induced landslides to long-term slope erosion and slope-failure hazards in seismically active regions. Geomorphology **10** : 265–284. DOI: 10.1016/0169-555X(94)90021-3

Kemeny J. 2005. Time-dependent drift degradation due to the progressive failure of rock bridges along discontinuities. International Journal of Rock Mechanics and Mining Sciences **42** : 35–46. DOI: 10.1016/j.ijrmms.2004.07.001

Korup O, Clague JJ, Hermanns RL, Hewitt K, Strom AL, Weidinger JT. 2007. Giant landslides, topography, and erosion. Earth and Planetary Science Letters **261** : 578–589. DOI: 10.1016/j.epsl.2007.07.025

Kromer RA, Abellán A, Hutchinson DJ, Lato M, Chanut M, Dubois L, Jaboyedoff M. 2017a. Automated terrestrial laser scanning with near-real-time change detection – monitoring of the Séchilienne landslide. : 293–310. DOI: 10.5194/esurf-5-293-2017

Kromer RA, Hutchinson DJ, Lato MJ, Gauthier D, Edwards T. 2015. Identifying rock slope failure precursors using LiDAR for transportation corridor hazard management. Engineering Geology **195** : 93–103. DOI: 10.1016/j.enggeo.2015.05.012

Kromer RA, Rowe E, Hutchinson J, Lato M, Abellán A. 2017b. Rockfall risk management using a pre-failure deformation database. Landslides DOI: 10.1007/s10346-017-0921-9

Lajtai E, Lajtai V. 1974. The evolution of brittle fracture in rocks. Journal of the Geological Society **130** : 1–16. DOI: 10.1144/gsjgs.130.1.0001

Lamp JL, Marchant DR, Mackay SL, Head JW. 2017. Thermal stress weathering and

the spalling of Antarctic rocks. Journal of Geophysical Research: Earth Surface **122** : 3–24. DOI: 10.1002/2016JF003992

Leith K, Moore JR, Amann F, Loew S. 2014a. In situ stress control on microcrack generation and macroscopic extensional fracture in exhuming bedrock. Journal of Geophysical Research: Solid Earth **119** : 594–615. DOI: 10.1002/2012JB009801

Leith K, Moore JR, Amann F, Loew S. 2014b. Subglacial extensional fracture development and implications for Alpine Valley evolution. Journal of Geophysical Research: Earth Surface **119** : 62–81. DOI: 10.1002/2012JF002691

Leroueil S. 2001. Natural slopes and cuts: movement and failure mechanisms. Geotechnique **51** : 197–243.

Lim M, Rosser NJ, Allison RJ, Petley DN. 2010. Erosional processes in the hard rock coastal cliffs at Staithes, North Yorkshire. Geomorphology **114** : 12–21. DOI: 10.1016/j.geomorph.2009.02.011

Loew S, Gschwind S, Gischig V, Keller-signer A, Valenti G. 2016. Monitoring and early warning of the 2012 Preonzo catastrophic rockslope failure. Landslides DOI: 10.1007/s10346-016-0701-y

Main IG. 2000. A damage mechanics model for power-law creep and earthquake aftershock and foreshock sequences. Geophysical Journal International **142** : 151–161. DOI: 10.1046/j.1365-246X.2000.00136.x

Martel SJ. 2006. Effect of topographic curvature on near-surface stresses and application to sheeting joints. Geophysical Research Letters **33** DOI: 10.1029/2005GL024710

Martin CD, Chandler NA. 1994. The progressive fracture of Lac du Bonnet granite. International Journal of Rock Mechanics and Mining Sciences and **31** : 643–659. DOI: 10.1016/0148-9062(94)90005-1

Matsuoka N, Sakai H. 1999. Rockfall activity from an alpine cliff during thawing periods. Geomorphology **28** : 309–328.

Messenzehl K, Meyer H, Otto J, Hoffmann T, Dikau R. 2017. Regional-scale controls on the spatial activity of rockfalls (Turtmann Valley , Swiss Alps) — A multivariate modeling approach. Geomorphology **287** : 29–45. DOI: 10.1016/j.geomorph.2016.01.008

Migon P. 2010. Mass movement and landscape evolution in weathered granite and gneiss terrains. Geological Society, London, Engineering Geology Special Publications **23** : 33–45. DOI: 10.1144/EGSP23.4

Mitchell TM, Faulkner DR. 2009. The nature and origin of off-fault damage surrounding strike-slip fault zones with a wide range of displacements: A field study from the Atacama fault system, northern Chile. Journal of Structural Geology **31** : 802–816. DOI: 10.1016/j.jsg.2009.05.002

Mol L, Viles HA. 2012. The role of rock surface hardness and internal moisture in tafoni development in sandstone. Earth Surface Processes and Landforms **37** : 301–314. DOI: 10.1002/esp.2252

Moore JR, Gischig V, Katterbach M, Loew S. 2011. Air circulation in deep fractures and the temperature field of an alpine rock slope. Earth Surface Processes and Landforms **36** : 1985–1996. DOI: 10.1002/esp.2217

Moore JR, Sanders JW, Dietrich WE, Glaser SD. 2009. Influence of rock mass strength on the erosion rate of alpine cliffs. Earth Surface Processes and Landforms **34** : 1339–1352. DOI: 10.1002/esp.1821

Moses C, Robinson D, Barlow J. 2014. Methods for measuring rock surface weathering and erosion: A critical review. Earth-Science Reviews **135** : 141–161. DOI: 10.1016/j.earscirev.2014.04.006

Mottershead D. 2013. Coastal Weathering. In Treatise on geomorphology: Weathering and soils geomorphology , . Elsevier: London; 228–244.

Nicholson DT. 2001. Pore properties as indicators of breakdown mechanisms in experimentally weathered limestones. Earth Surface Processes and Landforms **26** : 819–838. DOI: 10.1002/esp.228

Oda M, Takemura T, Aoki T. 2002. Damage growth and permeability change in triaxial compression tests of Inada granite. Mechanics of Materials **34** : 313–331. DOI: 10.1016/S0167-6636(02)00115-1

Perras MA, Diederichs MS. 2014. A review of the tensile strength of rock: concepts and testing. Geotechnical and Geological Engineering **32** : 525–546. DOI: 10.1007/s10706-014-9732-0

Petley DJDNDJ, Higuchi T, Petley DJDNDJ, Bulmer MH, Carey J. 2005. Development of progressive landslide failure in cohesive materials. Geology **33** : 201–204. DOI: 10.1130/G21147.1

Qi J, Sui W, Liu Y, Zhang D. 2015. Slaking process and mechanisms under static wetting and drying cycles slaking tests in a red strata mudstone. Geotechnical and Geological Engineering **33** : 959–972. DOI: 10.1007/s10706-015-9878-4

Rihosek J, Bruthans J, Masin D, Filippi M, Carling GT, Schweigstillova J. 2016. Gravity-induced stress as a factor reducing decay of sandstone monuments in Petra, Jordan. Journal of Cultural Heritage **19** : 415–425. DOI: 10.1016/j.culher.2015.10.004

Robinson DA, Williams RBG, Williams RGB. 1982. Salt weathering of rock specimens of varying shape. Area **14** : 293–299.

Rosser N, Lim M, Petley D, Dunning S, Allison R. 2007. Patterns of precursory rockfall prior to slope failure. Journal of Geophysical Research **112** DOI: 10.1029/2006JF000642

Rosser NJ, Brain MJ, Petley DN, Lim M, Norman EC. 2013. Coastline retreat via progressive failure of rocky coastal cliffs. Geology **41** : 939–942. DOI: 10.1130/G34371.1

Royan MJ, Abellan A, Vilaplana JM. 2015. Progressive failure leading to the 3 December 2013 rockfall at Puigcercos scarp (Catalonia, Spain). Landslides **12** : 585–595. DOI: 10.1007/s10346-015-0573-6

Røyne A, Jamtveit B, Mathiesen J, Malthe-Sørenssen A. 2008. Controls on rock weathering rates by reaction-induced hierarchical fracturing. Earth and Planetary Science Letters **275** : 364–369. DOI: 10.1016/j.epsl.2008.08.035

Sass O. 2005. Spatial patterns of rockfall intensity in the northern Alps. Zeitschrift fur Geomorphologie **138** : 51–65.

Slavík M, Bruthans J, Filippi M, Schweigstillová J, Falteisek L, Řihošek J. 2017. Biologically-initiated rock crust on sandstone: Mechanical and hydraulic properties and resistance to erosion. Geomorphology **278** : 298–313. DOI: 10.1016/j.geomorph.2016.09.040

Stock GM, Martel SJ, Collins BD, Harp EL. 2012. Progressive failure of sheeted rock slopes: the 2009-2010 Rhombus Wall rock falls in Yosemite Valley, California, USA. Earth Surface Processes and Landforms **37** : 546–561. DOI: 10.1002/esp.3192

Thomson BJ, Hurowitz JA, Baker LL, Bridges NT, Lennon AM, Paulsen G, Zacny K. 2014. The effects of weathering on the strength and chemistry of Columbia River Basalts and their implications for Mars Exploration Rover Rock Abrasion Tool (RAT) results. Earth and Planetary Science Letters **400** : 130–144. DOI: 10.1016/j.epsl.2014.05.012

de Vilder SJ, Rosser NJ, Brain MJ. 2017. Forensic analysis of rockfall scars. Geomorphology **295** DOI: 10.1016/j.geomorph.2017.07.005

Viles H. 2013a. Linking weathering and rock slope instability: non-linear perspectives. Earth Surface Processes and Landforms **38** : 62–70. DOI: 10.1002/esp.3294

Viles H. 2013b. Synergistic weathering processes. In Treatise on geomorphology: Weathering and soils geomorphology , . Elsevier: London; 12–26.

Viles H, Goudie A, Grab S, Lalley J. 2011. The use of the Schmidt Hammer and Equotip for rock hardness assessment in geomorphology and heritage science: a comparative analysis. Earth Surface Processes and Landforms **36** : 320–333. DOI: 10.1002/esp.2040

Viles H, Messenzehl K, Mayaud J, Coombes M, Bourke M. 2018. Stress histories control rock-breakdown trajectories in arid environments. Geology : 3–6.

Viles HA. 2005. Microclimate and weathering in the central Namib Desert, Namibia. Geomorphology **67** : 189–209. DOI: 10.1016/j.geomorph.2004.04.006

Voigtländer A, Leith K, Krautblatter M. 2018. Subcritical crack growth and progressive failure in Carrara Marble under wet and dry conditions. Journal of Geophysical Research: Solid Earth DOI: 10.1029/2017JB014956

Warke PA. 2007. Complex weathering in drylands: Implications of 'stress' history for rock debris breakdown and sediment release. Geomorphology **85** : 30–48. DOI: 10.1016/j.geomorph.2006.03.038

Williams JG, Rosser NJ, Hardy RJ, Brain MJ, Afana AA. 2018. Optimising 4-D surface change detection : an approach for capturing rockfall magnitude – frequency. Earth Surface Dynamics **6** : 101–119.

Yatsu E. 1988. The Nature of Weathering: An Introduction . Sozosha: Tokyo, Japan

Zhang BY, Zhang JH, Sun GL. 2015. Deformation and shear strength of rock fill materials composed of soft siltstones subjected to stress, cyclical drying/wetting and temperature variations. Engineering Geology **190** : 87–97. DOI: 10.1016/j.enggeo.2015.03.006

Zoback MD, Byerlee JD. 1975. The effect of microcrack dilatancy on the permeability of westerly granite. Journal of Geophysical Research **80** : 752–755. DOI: 10.1029/JB080i005p00752

Acknowledgments

The authors gratefully acknowledge support for this research from ICL Fertilizers (UK) Ltd. We thank Neil Tunstall and Chris Longley for help with laboratory testing, Dave Hodgson for help with the installation of the laboratory and field experiments, Sam Waugh for help with field monitoring, Simon Varley and Richard Boothroyd for help with sample collection, and Zuzanna Swirad for help with laboratory monitoring.

Figure 1. a) Example siltstone sample core. b) Example sandstone sample core. Both cores are 96 mm high, and 48 mm in diameter.

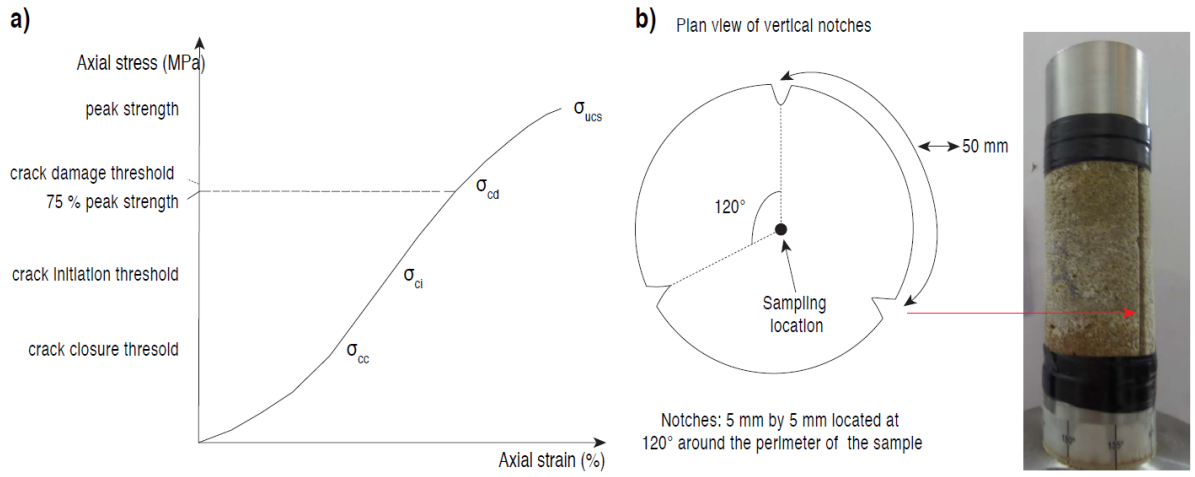

Figure 2. Detail of sample modifications for a) preloaded (*P*) and b) geometrically-altered (*G*) samples. a) Stress-strain curve showing the different stages of micro-crack development under conditions of uniaxial compression (adapted from: Eberhardt et al., 1998). Samples were preloaded to 75% of peak strength in order to exceed the crack initiation threshold but not exceed that of the crack damage threshold. b) Geometry of notches cut into *G* samples, showing the plan view and an example notch within a sandstone core.

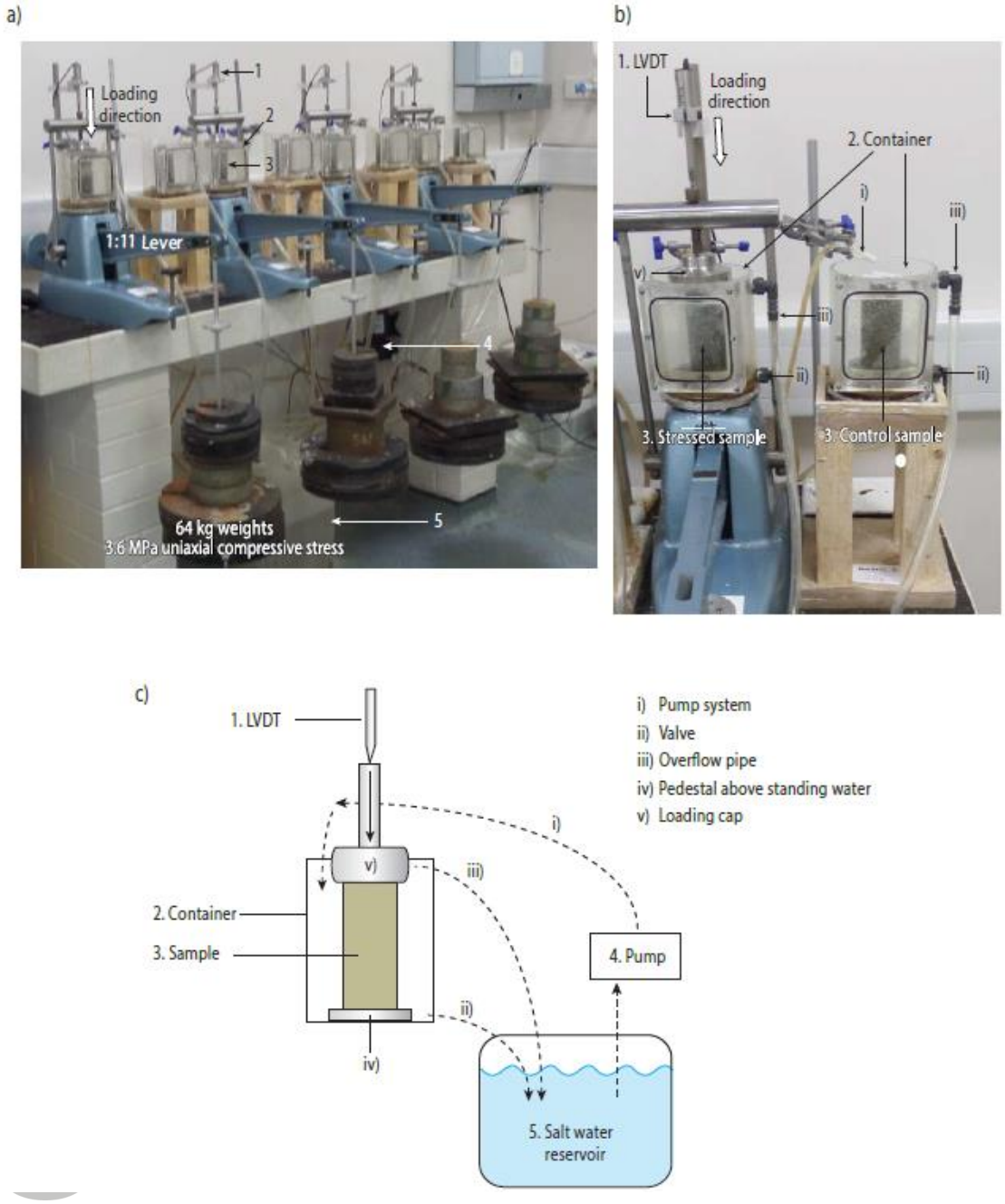

Figure 3. Detail of the laboratory weathering set-up, showing modified oedometers that subjected stressed samples to constant vertical compressive stress and corresponding control (non-stressed) samples (a and b). Vertical compressive stress is applied by fixed hanging weights and a lever system (a). The saltwater wetting and drying system is evident in a) and summarised conceptually in c). The system

operates by pumping water into the containers via a pipe (i) from the saltwater reservoir, and draining via a valve (ii) after 30 minutes of inundation. Over-topping of the containers was prevented through the use of an overflow pipe (iii). A small amount of standing water was present below the valve line within the container, and so samples were placed on a pedestal (iv) to ensure that they were located above the standing water to allow full drainage.

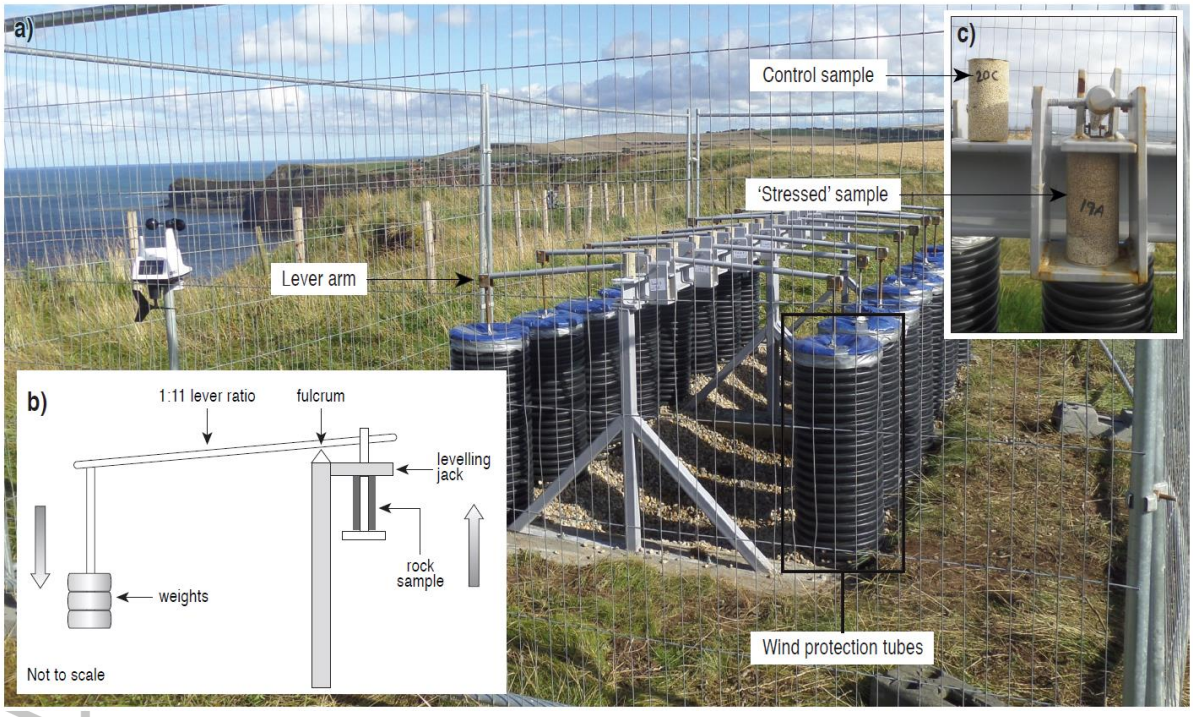

Figure 4. Photograph (a) and schematic summary (b) of the field compression apparatus used to place samples under a constant vertical compressive stress. Non-stressed samples were placed on top of the beam (c), while 'stressed' samples were placed under load using a simple lever system (c, d). The weights for each lever arm were contained within protective tubes to prevent the hanging weights from moving due to wind (a). Vertical compressive stress was applied to samples via level system (b). Samples were compressed against the levelling jack when weights were applied on the opposite lever arm.

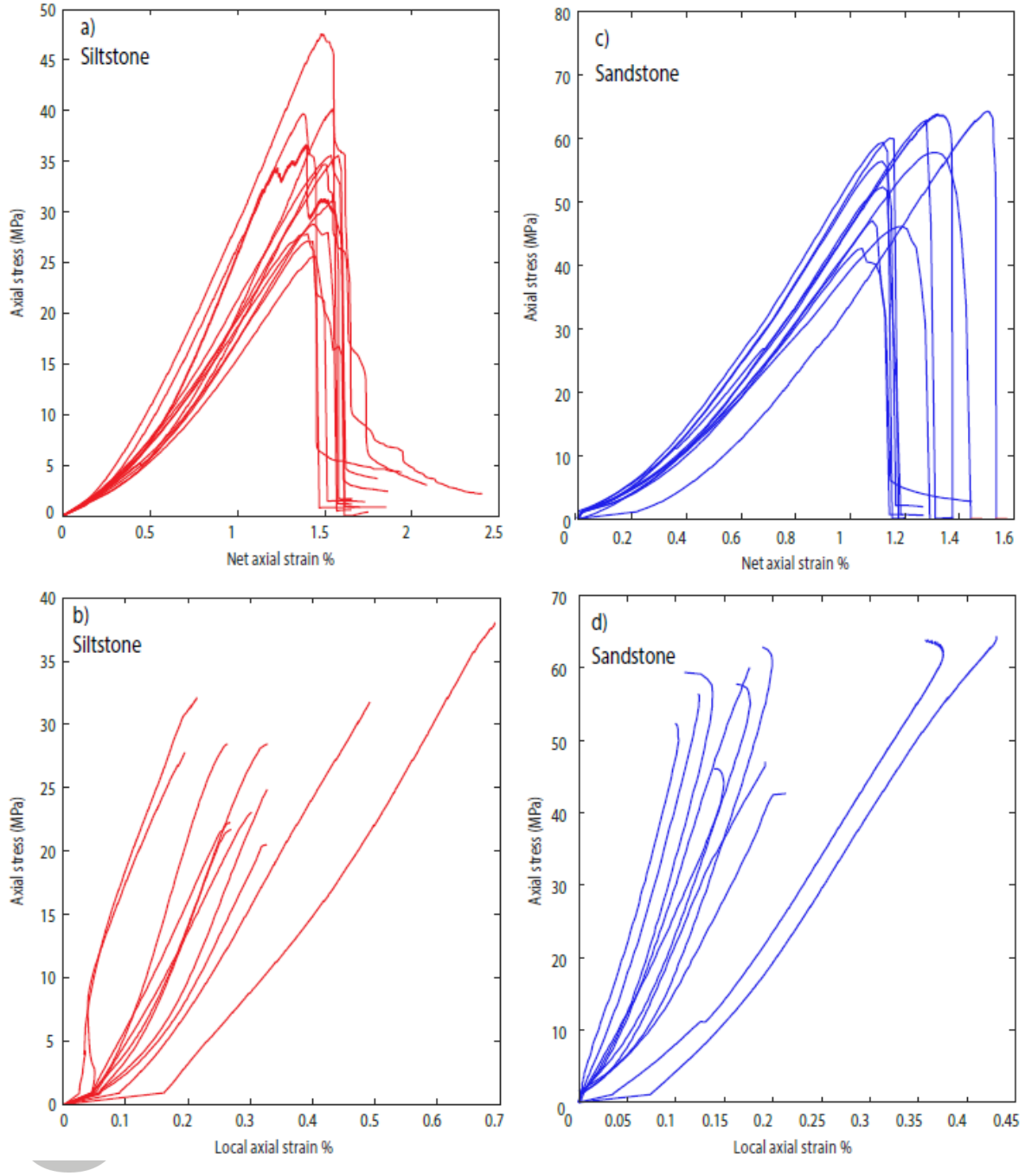

Figure 5. Stress-strain curves for unconfined compression tests on siltstone (a and b) and sandstone (c and d) samples for baseline property characterisation. a) and c) display net axial strain response; b) and d) display local (LVDT) strain response.

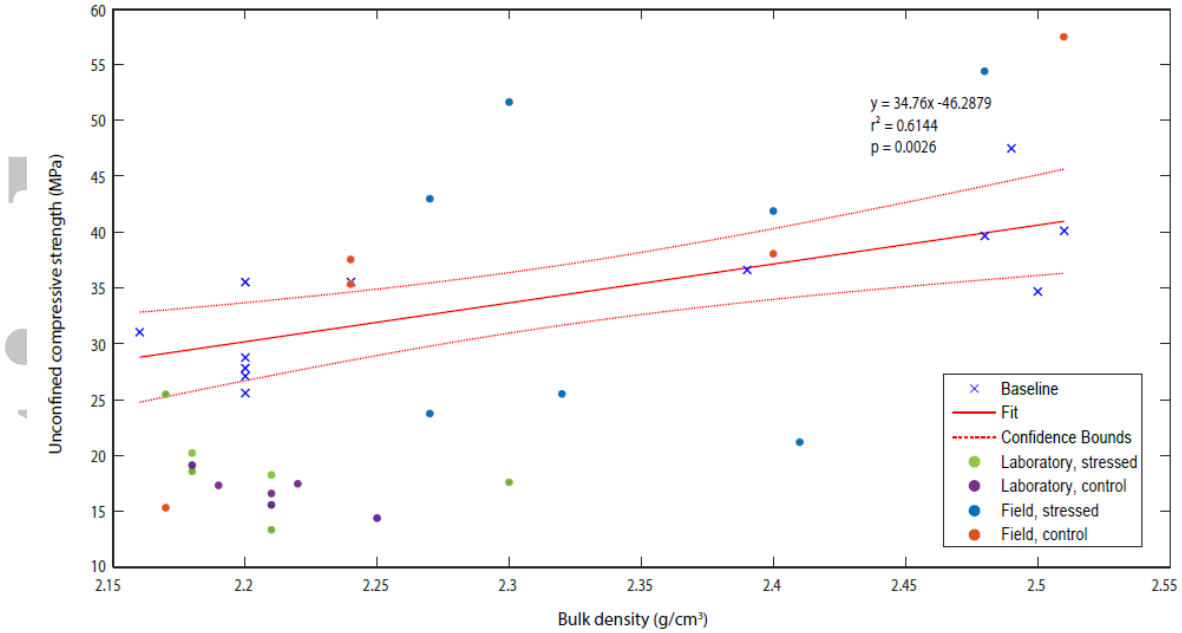

Figure 6. Scatter plot of UCS values against initial bulk density values for siltstone samples. The modelled regression envelope (fit plus 95% confidence bounds) and statistical summary information represent samples used for baseline characterisation. Results for samples weathered during field and laboratory experiments which plot outside of these bounds are considered to significantly different to baseline UCS values.

Figure 7. Photographs of weathered samples taken during monitoring experiments. a) Siltstone sample displaying slaking, with detached fragments evident around the base of the container. b) Siltstone core displaying an incipient slaking event characterised by a vertical shallow crack with a narrow aperture. c) Siltstone sample with a 'powdery' surface to touch, with many individual grains at the base of the core. d) Siltstone sample with multiple sub-horizontal cracks at the top and mid-point of the core. e) A sandstone sample with modified geometry *(G)* displaying iron leaching. f) Sandstone sample displaying an area of concentrated grain loss. a), b), and e) were

subjected to laboratory weathering conditions. c), d) and f) were subjected to field weathering conditions.

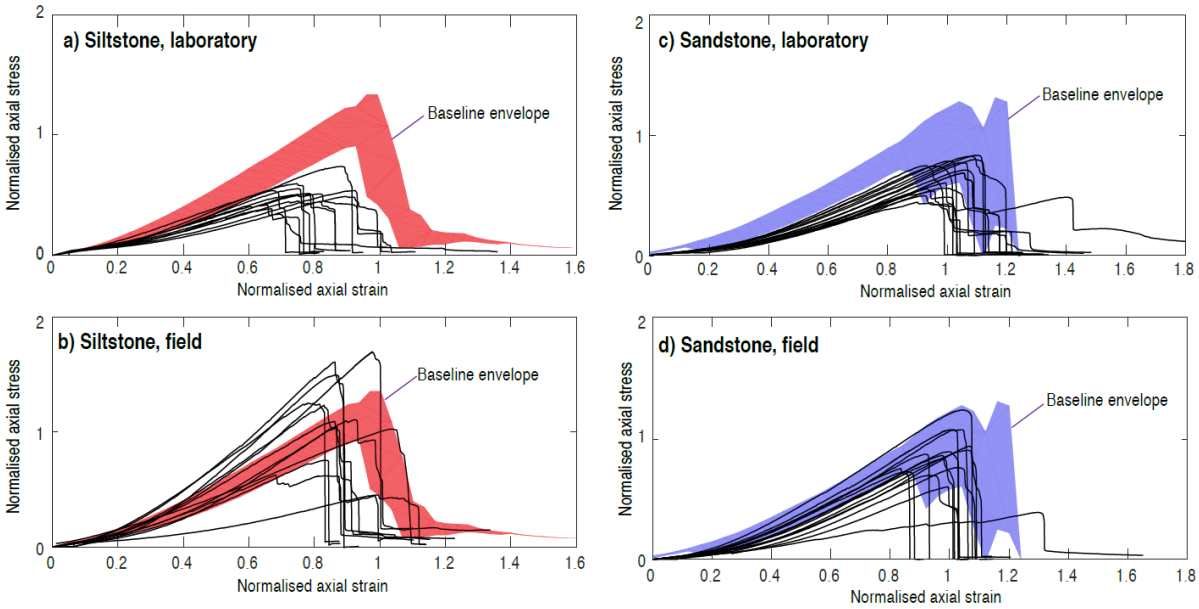

Figure 8. Normalised stress-strain curves for UCS tests of siltstone (a and b, laboratory and field respectively) and sandstone (c and d, laboratory and field respectively) samples following the completion of weathering experiments. Normalised values of 1 are equivalent to the mean UCS and strain-at-failure values observed in baseline tests. The shaded areas represent the envelope of the range of baseline stress values for a given strain value.

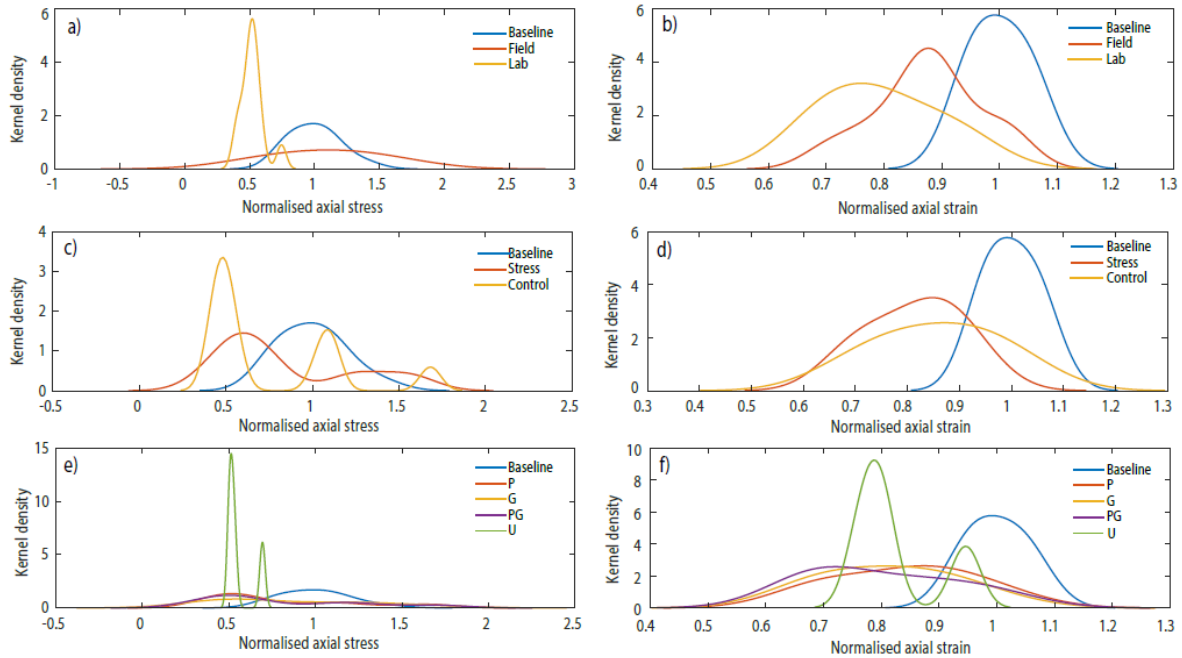

Figure 9. Kernel density plots displaying the distributions of normalised UCS and normalised axial strain at failure for siltstone samples of different groupings compared to baseline tests. Normalised values of 1 are equivalent to the mean UCS and strain-at-failure values observed in baseline tests. a) & b) Siltstone samples weathered in laboratory and field conditions compared to baseline tests. c) & d) 'Stressed' and 'control' siltstone samples compared to baseline tests. e) & f) Each sample pre-treatment group of siltstone subjected to weathering compared to baseline test results.

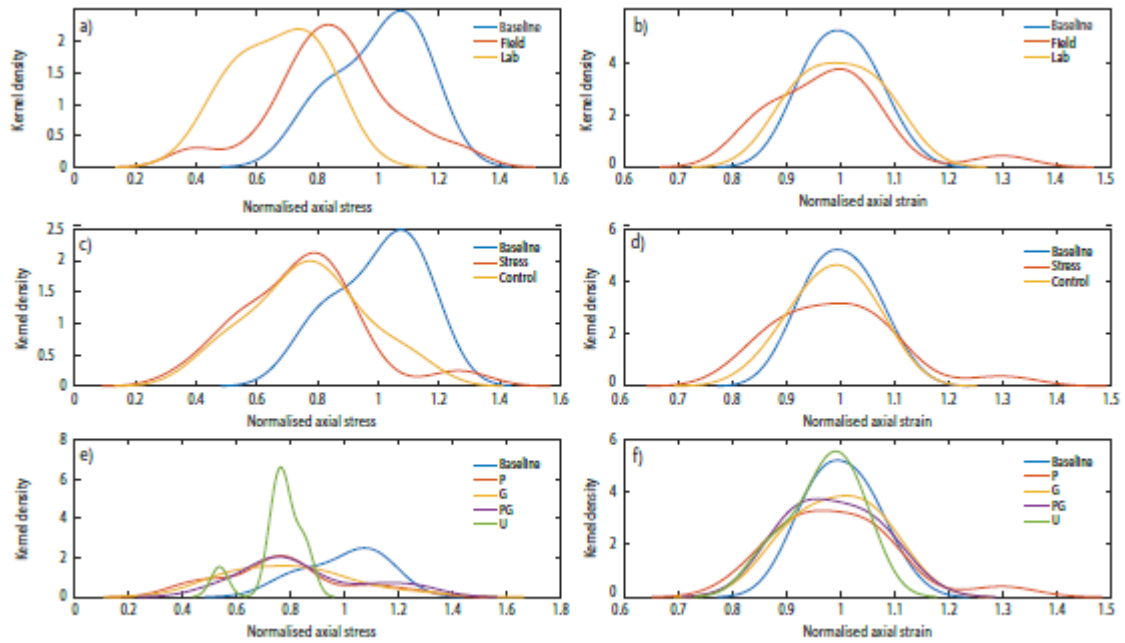

Figure 10. Kernel density plots displaying the distributions of normalised UCS and normalised axial strain at failure for sandstone samples of different groupings compared to baseline tests. Normalised values of 1 are equivalent to the mean UCS and strain-at-failure values observed in baseline tests. a) & b) Sandstone samples weathered in laboratory and field conditions compared to baseline tests. c) & d) 'Stressed' and 'control' sandstone samples compared to baseline tests. e) & f) Each sample pre-treatment group of sandstone subjected to weathering compared to baseline test results.

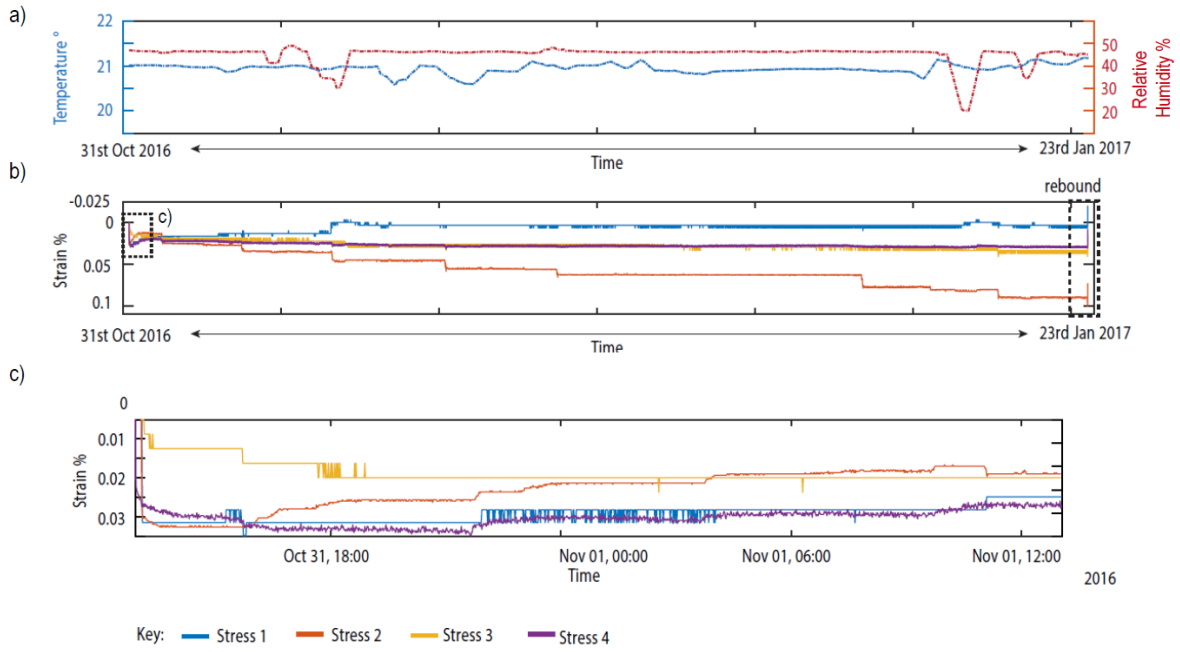

Figure 11. Strain response of four samples subjected to a constant uniaxial compressive load within the laboratory experiments. a) Daily averaged fluctuations in temperature and relative humidity within the climate-controlled laboratory over the duration of the experiment. b) Strain response for each of the four stressed siltstone samples within the laboratory experiments (Table 1). Stress 1 and 2 are *PG* samples, and Stress 3 and 4 are *G* samples. An increase in strain values reflects compression of the sample, while decreases in strain values reflect expansion of sample. Rebound occurred at the end of the experiment for all samples once the constant uniaxial compressive stress was removed. b) First 24 hours of experiment, displaying an initial compression for all samples, followed by either further compression as is the case for Stress 3, or expansion as seen for Stress 1, 2 and 4.

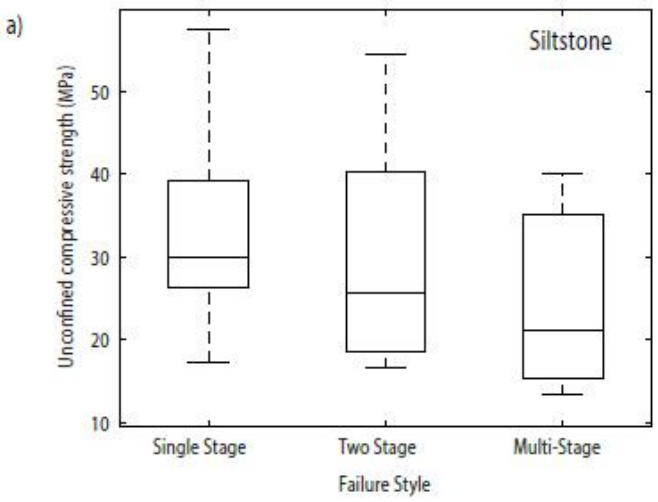

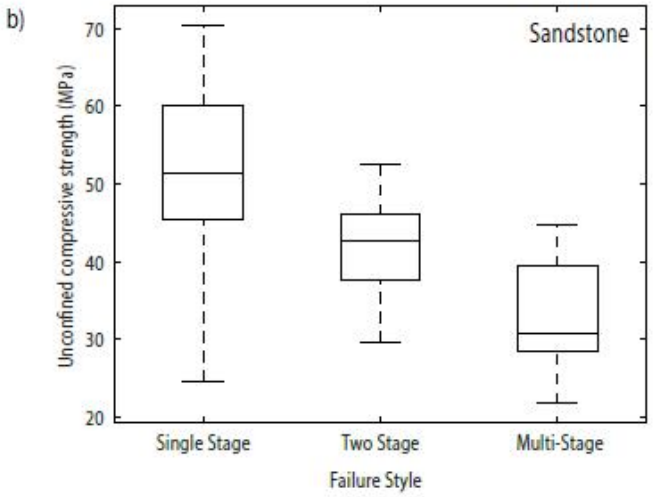

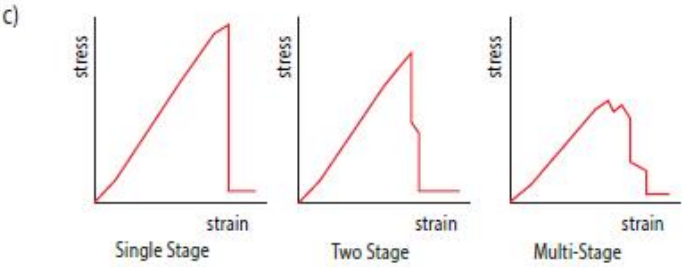

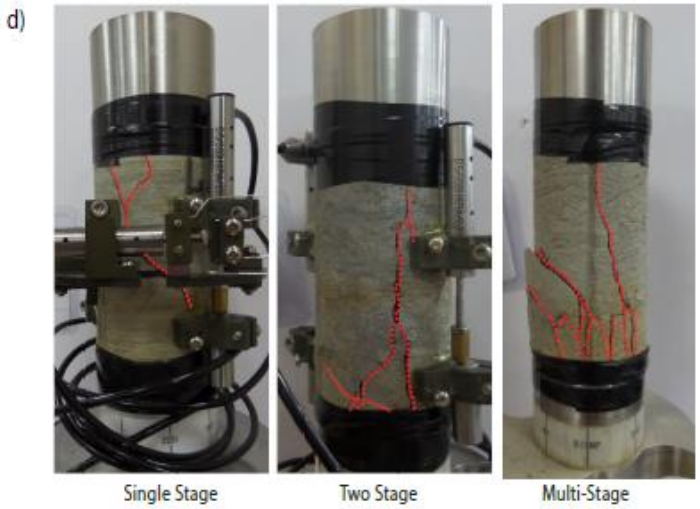

Figure 12. a) Boxplots displaying changes in UCS in relation to the number of stress-drop failure events observed for siltstone samples. b) Boxplots displaying changes in UCS in relation to the number of stress-drop failure events observed for sandstone samples. c) Conceptual diagrams of typical stress-strain plots associated with differences in the number of stress-drop failure events. d) Photographs of typical failure styles and the associated degree of fragmentation associated with differences in the number of stress-drop failure events.

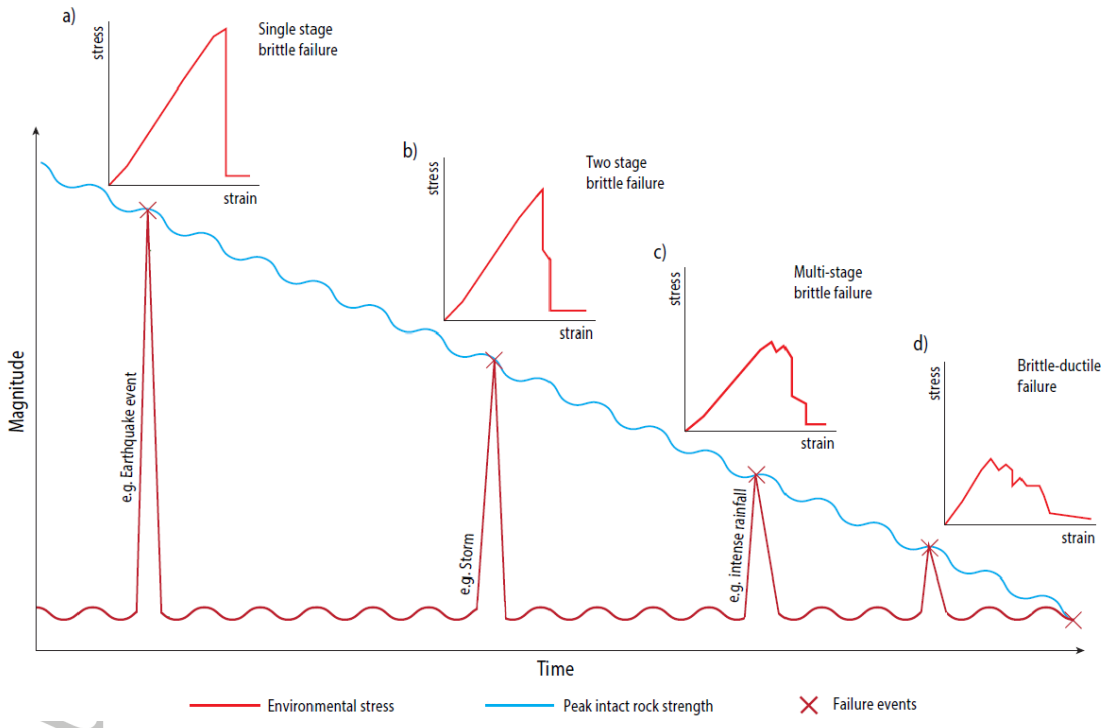

Figure 13. Conceptual diagram of the impact of incremental strength decrease over time in response to environmental conditions (modified from: Gunzburger et al., 2005). Over time, as rock strength decreases the failure style will transition from a purely brittle failure (a) to a multi-stage (c) and brittle-ductile failure (d). Each stress-strain curve represents the type of failure style expected given the strength of the rock, with the loading events, such as earthquakes and storms, representing the required stresses necessary for failure to occur. As weathering proceeds, the magnitude of the event required to cause failure decreases.

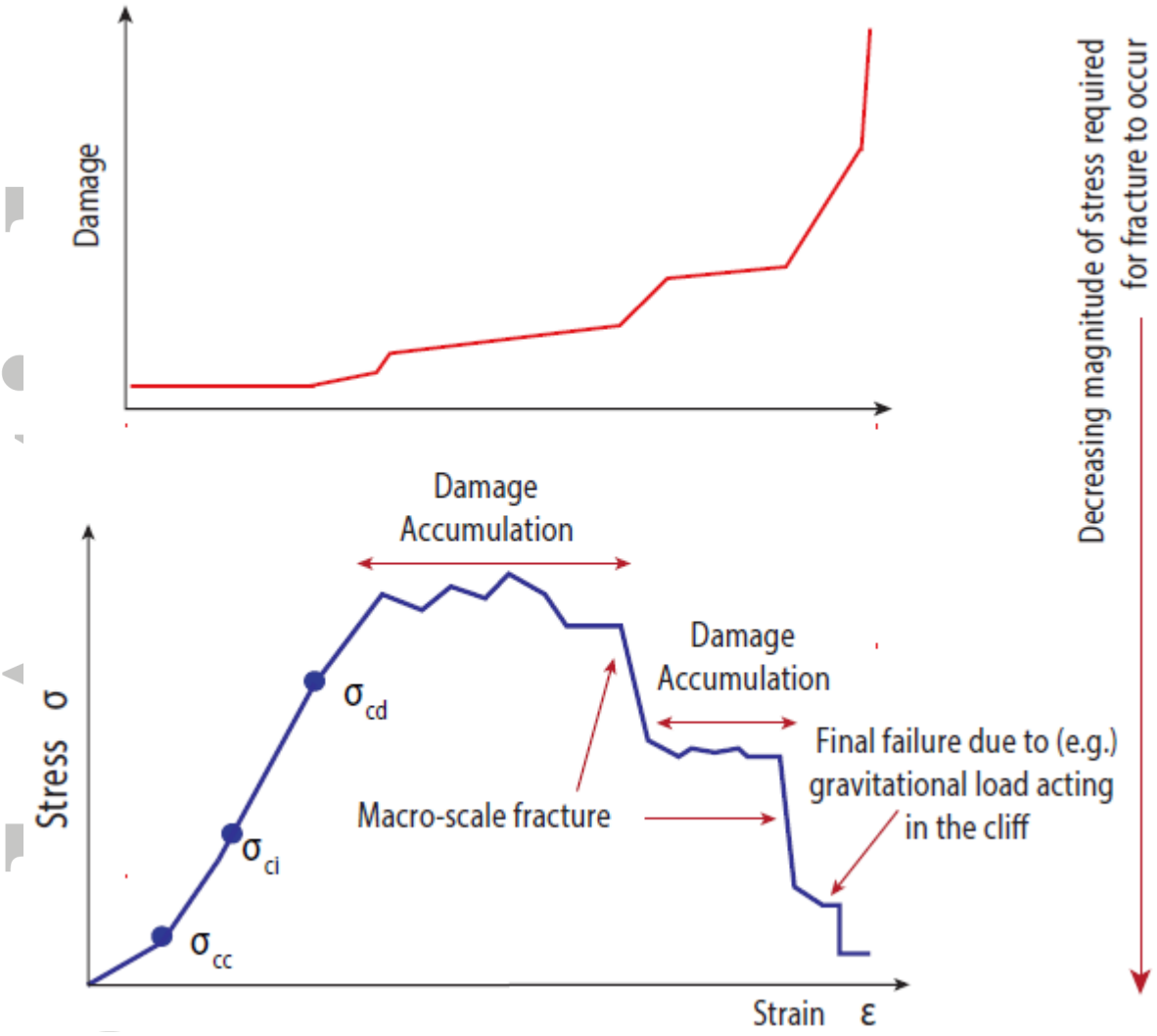

Figure 14. Conceptual stress-strain diagram of the stages and drivers of weathered brittle rock failure, displaying initial micro-crack initiation and propagation thresholds for intact rock (adapted from Eberhardt et al., 1998). For macro-scale fracture resulting in eventual final failure to occur, weathered rock bridges must experience sustained stress and strain, resulting in failure events.

Tables

Table 1: Sample types tested for each weathering experiment. For each of the sample types (e.g. *U, P, G, PG)*, two of the samples were placed under a constant vertical stress, while the other two samples were controls.

	Unmodified samples (U)	Pre-damaged samples (P)	Modified geometry samples (G)	Pre-damaged and modified geometry samples (PG)
Laboratory–Sandstone	4	4	4	4
Laboratory - Siltstone	4	4	4	4
Cliff – Sandstone	4	4	4	4
Cliff - Siltstone	4	4	4	4

Table 2: Baseline geotechnical characteristics derived from UCS testing.

	UCS (MPa)		Mean bulk density (g cm^{-3})		Mean Young's modulus (GPa)		Mean axial strain at failure (%)				Brittle failure events
							Machine strain		Local strain		
	Mean	Standard deviation	Mean	Standard deviation	Mean	Standard deviation	Mean	Standard deviation	Mean	Standard deviation	Mean
Siltstone	34.15	6.43	2.31	0.15	8.99	3.2	1.47	0.07	0.46	0.21	1.7
Sandstone	55.69	7.61	2.4	0.04	5.69	0.86	1.25	0.07	0.24	0.14	1

Table 3: Geotechnical characteristics obtained from UCS testing of both lithologies following laboratory weathering experiments.

Lithology	Ambient stress conditions	Sample type	No. of samples	Mean values				
				UCS (MPa)	Net axial strain at failure (%)	Local axial strain at failure (%)	Young's Modulus (GPa)	Brittle failure events
Siltstone	Control	All	6	16.72 (±1.64)	1.15 (±0.13)	0.38 (±0.17)	3.41 (±1.73)	2
		U	2	18.73	1.17	0.24	5.40	2
		P	1	16.57	1.36	NA*	NA*	2
		G	1	15.55	1.14	0.27	2.18	3
		PG	2	16.74	1.02	0.20	2.66	3
	Stressed	All	6	18.89 (±3.95)	1.19 (±0.16)	0.27 (±0.18)	1.69 (±0.03)	2
		U	1	18.23	1.39	NA*	NA*	1
		P	1	20.19	1.13	NA*	NA*	2
		G	2	22.00	1.18	0.15	1.70	3
		PG	2	15.45	1.12	0.12	1.70	2
Sandstone	Control	All	8	35.76 (±7.5)	1.23 (±0.09)	0.22 (±0.2)	6.58 (±1.47)	2
		U	2	27.73	1.18	0.13	8.60	2
		P	2	31.11	1.20	0.22	6.67	3
		G	2	42.00	1.34	0.15	5.85	2
		PG	2	42.21	1.22	0.37	5.22	3
	Stressed	All	8	38.73 (±7.32)	1.25 (±0.09)	0.27 (±0.16)	5.49 (±0.38)	2
		U	2	42.73	1.33	0.28	5.78	2
		P	2	39.39	1.31	0.28	5.47	2
		G	2	36.01	1.14	0.33	5.74	2
		PG	2	36.79	1.23	0.21	4.96	2

*No local axial data and associated Young's modulus values were obtained.

Table 4: Geotechnical characteristics obtained from UCS testing of sandstone and siltstone samples following field weathering experiments.

Lithology	Ambient stress conditions	Sample type	No. of samples	Mean values: UCS (MPa)	Net axial strain at failure (%)	Local axial strain at failure (%)	Young's modulus (GPa)	Brittle failure stages
Siltstone	Control	All	5	36.71 (±14.93)	1.40 (±0.09)	0.26 (±0.17)	5.00 (±1.52)	2
		U	1	37.51	1.30	NA*	NA	2
		P	2	25.30	1.41	0.15	3.93	3
		G	0	-	-	-	-	-
		PG	2	47.73	1.44	0.38	6.08	2
	Stressed	All	7	37.30 (±13.74)	1.21 (±0.1)	0.29 (±0.17)	3.63 (±2.79)	2
		U	1*	23.72	1.12	0.41	1.81	2
		P	2	39.92	1.28	0.25	0.73	1
		G	2	47.27	1.24	0.24	6.45	3
		PG	2	31.50	1.14	0.27	5.53	3
Sandstone	Control	All	8	49.93 (±7.84)	1.23 (±0.08)	0.22 (±0.16)	7.07 (±2.39)	2
		U	2	45.31	1.25	0.25	6.69	2
		P	2	52.51	1.16	0.21	6.25	2
		G	2	51.51	1.28	0.14	10.47	2
		PG	2	50.41	1.21	0.27	4.89	2
	Stressed	All	8	44.53 (±14.16)	1.23 (±0.19)	0.17 (±0.14)	6.90 (±0.86)	2
		U	2	43.68	1.14	0.04	7.40	2
		P	2	31.99	1.33	0.17	6.01	3
		G	2	42.44	1.21	0.24	6.37	2
		PG	2	59.99	1.22	0.23	7.85	1

*No local axial data and associated Young's modulus values were obtained.

Table 5: Strength properties of samples weathered in each environmental setting and test conditions. Absolute and percentage differences from equivalent baseline samples are displayed. Negative values are weaker than corresponding baseline values, and positive values are stronger.

		UCS					Young's Modulus percent difference (%)**	Percent difference in net axial strain at failure (%)
		Mean (MPa)	Standard deviation (MPa)	Absolute difference (MPa)*	Percent difference (%)*	Statistical significance tests (*p values)*		
Siltstone	All samples	27.43	13.76	-5.25	-18.10	**<0.001**	-61.43	-16.62
	All field	37.10	13.57	2.21	5.23	0.583	-54.54	-12.55
	All lab.	17.81	3.10	-12.70	-41.36	**<0.001**	-69.70	-20.69
	Stressed	28.80	13.86	-4.33	-14.52	**0.043**	-66.82	-18.57
	Control	25.81	14.13	-6.34	-22.26	**0.035**	-54.96	-14.31
	U	19.17	3.06	-11.79	-38.28	**0.011**	-59.90	-17.45
	P	27.86	14.94	-5.95	-20.38	0.099	-74.10	-10.94
	G	29.6	14.88	-3.64	-12.70	0.734	-59.87	-17.52
	PG	27.85	16.01	-6.94	-22.84	0.898	-57.03	-19.78
Sandstone	All samples	42.24	10.70	-13.45	-24.15	**<0.001**	14.43	-1.10
	All field	47.23	11.40	-8.46	-15.19	**0.042**	22.80	-1.81
	All lab.	37.24	7.32	-18.45	-33.12	**<0.001**	6.06	-0.38
	Stressed	41.63	11.29	-14.06	-25.25	**0.001**	8.88	-0.66
	Control	42.85	10.41	-12.84	-23.06	**0.001**	19.98	-1.53
	U	42.00	5.49	-13.69	-24.60	**<0.001**	25.01	-3.24
	P	42.92	13.15	-12.77	-22.93	**0.001**	7.18	0.23
	G	44.11	11.77	-11.58	-20.80	**0.002**	24.88	0.11
	PG	47.10	13.12	-8.59	-15.42	0.089	0.66	-1.49

*Difference from mean baseline values.
**Calculated from local strain data